Implementing plant hydraulics in the Community Land Model

Daniel Kennedy[1], **Sean Swenson**[2], **Keith W. Oleson**[2], **David M. Lawrence**[2], **Rosie Fisher**[2], **Pierre Gentine**[1]

[1]Columbia University, New York, NY 10027 USA
[2]National Center for Atmospheric Research, Table Mesa Drive, Boulder, Colorado, USA

Key Points:

- A simplified soil-plant-atmosphere continuum model based on hydraulic theory is implemented in the Community Land Model (version 5).
- Prognostic leaf water potential replaces soil matric potential as the basis for stomatal conductance water stress.
- Prognostic root water potential is used to implement hydraulic root water uptake, replacing the heuristic soil 'wilting' point.

Corresponding author: Daniel Kennedy, `djk2120@columbia.edu`

Abstract

= enter abstract here =

1 Introduction

Trees face emerging climate change risk globally [*Allen et al.*, 2010; *Anderegg et al.*, 2013a]. In addition to stress from soil moisture drought, vegetation is susceptible to increasing atmospheric demand [*Restaino et al.*, 2016; *Novick et al.*, 2016a; *Lemordant et al.*, 2018]. Increases in vapor pressure deficit (VPD) are occurring with global warming [*Ficklin and Novick*, 2017; *Seager et al.*, 2015], and are associated with impacts on vegetation such as large-scale die-off [*Williams et al.*, 2013; *Mcdowell and Allen*, 2015]. Understanding vegetation response is important both for discerning future climate impacts on forests and for modeling feedbacks to the carbon and hydrological cycles [*Lemordant et al.*, 2018]. Significant uncertainty remains in Earth System model predictions of the carbon cycle caused by the response of vegetation to changes in hydroclimate [*De Kauwe et al.*, 2017; *Friedlingstein et al.*, 2014; *Trugman et al.*, 2018].

Plant water stress parameterizations are used by Earth System Models to determine the regulation of surface fluxes (photosynthesis, transpiration) by vegetation in response to water fluctuations [*Egea et al.*, 2011; *Verhoef and Egea*, 2014]. These parameterizations, which relate a metric of soil moisture status to leaf gas exchange, are widely used to define the response of stomatal conductance to vegetation water status, serving to attenuate transpiration, photosynthesis, and root water uptake with drying. Because vegetation water use strategies modulate carbon uptake, creating a close coupling between the Earth System's carbon and hydrological cycles [*Green et al.*, 2017], the dynamics of the water stress representation in models have broad effects on critical land surface processes [*Joetzjer et al.*, 2014], such as photosynthesis rates. On daily and weekly time scales, water stress parameterizations influence the partitioning of latent versus sensible heat, modifying the Bowen ratio [*Gentine et al.*, 2007, 2011]. This in turn feeds back onto surface and air temperature, through land-atmosphere feedbacks [*Bonan*, 2008; **?**]. On longer timescales vegetation water use strategies regulate the global carbon and water cycles [*De Kauwe et al.*, 2015].

Several recent studies have aimed at advancing the representation of water flow through the Soil-Plant-Atmosphere continuum (SPAC) in land-surface and ecosystem models [*Xu et al.*, 2016; *Christoffersen et al.*, 2016; *Sperry et al.*, 2017] by incorporating plant hydraulic theory. Explicit modeling of water flow through the vegetation adds complexity, but is consistent with evidence of dynamic regulation of vegetation water use in response to both soil and atmospheric drying [**?***Sperry et al.*, 1998; *Sperry and Love*, 2015]. Furthermore, because they are based on Darcy's Law, plant hydraulic models have a robust physical basis compared to models that utilize empirical water stress formulations. Plant hydraulic models involve new parameters, which presents challenges [*Drake et al.*, 2017], but plant hydraulic trait data are available [*Kattge et al.*, 2011; *Anderegg*, 2015a], providing constraints on parameter estimation. Such data have been shown to be informative of species vulnerability to drought [*Choat et al.*, 2012]. Likewise vegetation water status observations are now available from remote sensing platforms, at a scale that is directly comparable to model development [*Konings et al.*, 2016; *Grant et al.*, 2016] and therefore can be used to validate model results [*Momen et al.*, 2017; *Konings et al.*, 2017b].

In this study, we develop a new plant water stress parameterization based on hydraulic theory within the recently released Community Land Model, version 5 (CLM5, the land component of the Community Earth System Model version 2). We refer to this hydraulics-based implementation as the 'Plant Hydraulic Stress' (PHS) configuration. Previous versions of the CLM, similar to many Land Surface Models, employed an empirical β-form soil moisture stress function. Such functions lack a strong physical basis and have been shown to systematically overestimate the effect of soil moisture drought on evaporative fluxes [*Ukkola et al.*, 2016; *Bonan et al.*, 2014]. In Amazonia, which is the focus area of our model test

runs, studies suggest that the CLM (version 3.5) simultaneously underestimates the effect of experimental drought treatment [*Powell et al.*, 2013] and overestimates dry-season reductions in GPP [*Restrepo-Coupe et al.*, 2017].

PHS, by explicitly representing plant hydraulics, introduces modeled vegetation water potential (discretized into leaf, stem and root elements) into the CLM, as well as a physical model of water supply, from the soil through the vegetation substrate. Transpiration is attenuated in the model according to leaf water status, capturing dynamic vegetation water use regulation in response to both soil moisture and atmospheric evaporative demand. These changes in the parameterization framework have numerous implications, including:

1. Leaf water potential serves as a metric for plant water status instead of soil water or soil matric potential. As such, it reflects vegetation sensitivity to both soil and atmospheric drying, while serving as a diagnostic for excessive xylem tension and cavitation risk.
2. Modeling plant hydrodynamics allows representation of hydraulic redistribution [*Lee et al.*, 2005], as the flow respects Darcy's law and thus is always directed down gradients of water potentials.
3. Root water potential can be used to predict gradient-based root water uptake based on Darcy's law, replacing the previous empirical transpiration partitioning heuristic. This provides the means to vary, for example, the mean depth of extraction with changing soil water conditions.
4. Representation of a range of water use strategies (i.e. isohydricity and anisohydricity), improving the connection between plant carbon allocation and water availability.
5. Modeling vegetation water potential allows improved connection to remote sensing observations of vegetation water status (Vegetation Optical Depth) [*Konings et al.*, 2016].

To assess the new model formulation, we carried out site-level simulations at Caxiuanã National Forest in Brazil, which features a critical biome (terra-firme moist tropical evergreen forest) [*Fisher et al.*, 2006]. Starting in 2001, a plot at this site was subjected to an approximately 50% percent precipitation throughfall exclusion. Due to the large drop in soil moisture at the precipitation exclusion site, significant vegetation water stress regulation of transpiration and photosynthesis was observed at the site, providing an interesting test for the model [*Fisher et al.*, 2007].

In this paper we therefore:

1. Introduce the PHS theory and implementation in the CLM (Section 2)
2. Describe the details of the experiment setup
3. Analyze the dynamics of modeled water stress, root water uptake and soil moisture profiles (Section 4)
4. Compare PHS to the behavior of the previous CLM water stress configuration (Section 5)
5. Discuss the benefits and limitations of the new model (Section 5.7)

2 Model Description

This study uses CLM5 to compare two parameterizations of water stress (Sections 2.4.1 and 2.5.1) and root water uptake (Sections 2.4.2 and 2.5.2). The first parameterization, which we refer to as Soil Moisture Stress (SMS), deploys the CLM4.5 default root water uptake and water stress implementations within CLM5. The second is called Plant Hydraulic Stress (PHS); PHS is the default configuration of CLM5. In Sections 2.1-2.3, we describe components that the two configurations share in common. In Sections 2.4 and 2.5, we describe their differences.

2.1 Stomatal Conductance

CLM5 implements the Medlyn stomatal conductance model, which reconciles the empirical and optimal approaches to stomatal conductance [*Medlyn et al.*, 2011]. Such "optimal" stomatal model aims at maximizing photosynthesis relative to transpiration costs. Stomatal conductance of CO_2 (g_s) is directly related to net photosynthesis (A_n) and inversely related to the square root of the vapor pressure deficit near the leaf surface ($\sqrt{D}$) and the concentration of CO_2 at the leaf surface (C_a).

$$g_s = g_0 + \left(1 + \frac{g_1}{\sqrt{D}}\right)\frac{A}{C_a} \tag{1}$$

The model features two parameters g_0 (μmol / m^2 / s) and g_1 (kPa$^{0.5}$). The g_0 parameter is the minimum stomatal conductance, representing cuticular and epidermal losses (small). The g_1 parameter relates to the marginal water cost guiding the optimization of carbon assimilation. These parameters are plant functional type dependent.

While maximizing assimilation relative to water transpiration costs ($A - \lambda E$), the Medlyn model does not resolve concurrent limitations to stomatal conductance associated with declining soil water. To represent soil water stress, and its impact on leaf-gas exchange, land surface models typically include a 'water stress factor'.

2.2 Photosynthesis

The CLM5 photosynthesis model is described in detail in *Bonan et al.* [2011], *Thornton and Zimmermann* [2007], and *Oleson et al.* [2013]. Photosynthesis is limited by three factors: carboxylation-limitations, light-limitations, and export-limitations following *Farquhar et al.* [1980] and *Harley et al.* [1992]. Water stress (as discussed in the next section) is applied within the carboxylation-limited regime, by attenuating the maximum rate of carboxylation (V_{cmax}). The implementation extends *Sellers et al.* [1996a,b] with co-limitation following *Collatz et al.* [1991].

The CLM5 photosynthesis module, in its default configuration, is a two-big-leaf model, with a sunlit and shaded leaf for each plant functional type [*Thornton and Zimmermann*, 2007; *Dai et al.*, 2004; *Oleson et al.*, 2013]. The canopy fluxes module iterates the solution for leaf temperatures to satisfy the leaf surface energy balances on both sunlit and shaded leaves, in response to forcing conditions. Within this, the photosynthesis module further iterates to solve for stomatal conductance and intercellular CO_2 concentration, balancing stomatal flux of CO_2 with photosynthetic assimilation flux of CO_2 (see Supp Fig B.1 for a flow chart of these iterations).

2.3 Water stress factor

Uncertainty remains within the literature as to how and where to apply water stress factors to photosynthesis and/or stomatal conductance [*Zhou et al.*, 2013; *Novick et al.*, 2016b; *Sperry and Love*, 2015]. In the CLM, the water stress factor (f_w) multiplies the 'well-watered rate' of maximum carboxylation ($V_{cmax,ww}$) to effect water stress (as described in *Oleson et al.* [2013]).

$$V_{cmax} = f_w V_{cmax,ww} \tag{2}$$

Attenuating V_{cmax} is not the only method for incorporating a response to declining water availability. Other models opt to apply water stress directly to stomatal conductance, linking the stomatal conductance model slope parameter to soil moisture (e.g. *De Kauwe et al.* [2015]). However, *Lin et al.* [2018] found that only the intercept parameter and photosynthesis (through changes in light-use efficiency) were sensitive to soil moisture based on eddy-covariance observations and not the slope parameter. Furthermore *Zhou et al.* [2013] suggest

that changes in assimilation tend to exceed those predicted by modulating g_1 with soil moisture, but could be captured by changing V_{cmax}. These results would thus suggest that it is appropriate to modulate V_{cmax}. Other field studies, however, suggest that measured V_{cmax} at the leaf level does not change with drought [*Flexas et al.*, 2004]. On the other hand, the modeled V_{cmax} is a bulk measure of V_{cmax} and may implicitly account for mesophyll conductance changes [*Rogers et al.*, 2017], which has been shown to be water stress dependent [*Flexas et al.*, 2012].

For now, applying water stress through V_{cmax} seems well-supported, but future refinements may be appropriate. In this study, we preserve the method of applying water stress used in CLM4.5, while experimenting with how f_w responds to environmental conditions.

2.4 SMS (CLM4.5 default)

2.4.1 SMS Water Stress Factor

In SMS, the water stress f_w is calculated as the summation of a soil wilting factor (w_i) across the n soil layers, weighted by root fraction (r_i) [*Oleson et al.*, 2013]. The soil wilting factor is a bounded linear function of soil matric potential ($\psi_{soil,i}$). The function is defined by two parameters, the soil potential at which stomates fully open (ψ_o) and the value at which stomates are fully closed (ψ_c).

$$f_{w,\text{SMS}} = \sum_{i=1}^{n} r_i w_i \tag{3}$$

$$w_i = 0 \le \frac{\psi_{soil,i} - \psi_c}{\psi_o - \psi_c} \le 1 \tag{4}$$

2.4.2 SMS Root Water Uptake

The CLM features a vertically discretized soil column with variable soil layer thicknesses. The number of soil layers (n) can vary, depending on the depth to bedrock. Soil water movement in each soil layer is governed by Richards' equation, with root water uptake (q_i) incorporated as a sink term. Summed over the soil column, root water uptake is required to equal transpiration (T).

$$T = \sum_{i}^{n} q_i \tag{5}$$

In the SMS configuration, a heuristic function is used to determine q_i. Transpiration is partitioned among the soil layers based on the product of the root fraction and the wilting factor, which is then normalized by f_w so that 100

$$q_i = \frac{r_i w_i}{f_w} T \tag{6}$$

Substituting for w_i yields the SMS root water uptake equation as a function of the layer-i soil potential ($\psi_{soil,i}$).

$$q_i = \begin{cases} 0 & \text{if } \psi_{\text{soil},i} < \psi_c \\[2ex] \dfrac{T}{f_w} \dfrac{r_i}{\psi_o - \psi_c} \left(\psi_{\text{soil},i} - \psi_c \right) & \text{if } \psi_c \leq \psi_{\text{soil},i} \leq \psi_o \\[2ex] \dfrac{T}{f_w} r_i & \text{if } \psi_{\text{soil},i} > \psi_o \end{cases} \tag{7}$$

In the Darcy framework, water fluxes are the product of hydraulic conductance (k_i) and hydraulic gradient ($\Delta\psi$). Although SMS does not explicitly calculate hydraulic conductance, (7) can be used to define hydraulic analogs resulting from the transpiration partitioning heuristic function, allowing easier comparison to the PHS root water uptake implementation.

$$\begin{aligned} q_i &= -k_i \Delta\psi \\ \Delta\psi &= \psi_c - \psi_{\text{soil},i} \\ k_i &= \dfrac{T}{f_w} \dfrac{r_i}{\psi_o - \psi_c} \end{aligned} \tag{8}$$

$$\text{constrained by:} \quad \Delta\psi = \begin{cases} 0 & \text{if } \psi_{\text{soil},i} < \psi_c \\ \psi_c - \psi_o & \text{if } \psi_{\text{soil},i} > \psi_o \end{cases}$$

2.5 PHS (CLM5 default)

2.5.1 PHS Water stress factor

PHS introduces a new formulation of the water stress function, f_w, which is based on leaf water potential (ψ_{leaf}) instead of soil potential (described further in Section 2.5.6). The relationship is modeled with a sigmoidal function, subject to two parameters: the water potential at 50% loss of stomatal conductance (ψ_{50}) and a shape-fitting parameter (c_k).

$$f_{w,\text{PHS}} = 2^{-\left(\frac{\psi_{\text{leaf}}}{\psi_{50}} \right)^{c_k}} \tag{9}$$

Utilizing leaf water potential, instead of soil water potential, for drought stress introduces a new interpretation of vegetation water stress to the model. Leaf water potential is modulated by supply of sap to the leaves and by evaporative demand, as regulated by stomatal dynamics [*Novick et al.*, 2016b]. As a result, low soil water (bottom-up stress) induces stress due to limited water supply, but in addition, high atmospheric VPD can induce stress with the associated increases in the gradient in water potential across the plant xylem (top-down stress). This latter mechanism was absent from the previous water stress function (dependent on soil water potential only), by construction. Given the observed increase in VPD with global warming, it appears critical to include such mechanistic dependence of water stress. While the Medlyn stomatal conductance model does depend on VPD, the model does not (given constant g_1) reflect the risk of hydraulic failure [*Zhou et al.*, 2013]. The new stress factor formulation reflects the dual risks of soil moisture deficit and atmospheric demand on hydraulic safety [*Williams et al.*, 2013], requiring vegetation to avoid excessive xylem tension associated with risk of cavitation.

2.5.2 PHS Root Water Uptake

PHS implements an alternative to the SMS heuristic approach for root water uptake, using a mechanistic representation following Darcy's Law. Instead of a constant parameter (ψ_c) defining $\Delta\psi$, PHS implements a physical model of vegetation water potential (described

in Section 2.5.3). The water flux from a given soil layer is driven by the gradient between soil potential ($\psi_{\text{soil},i}$) and the water potential in the root collar (ψ_{root}), after accounting for the effects of gravity ($\rho g z_i$, where z_i is the soil layer depth). Hydraulic conductance across the soil and roots (k_{sr}) is modeled based on soil hydraulic properties and xylem vulnerability, accounting for both the path across the soil matrix and through the xylem conduits (details in Appendix B).

$$q_i = -k_{sr,i} \left(\psi_{\text{root}} - \psi_{\text{soil},i} + \rho g z_i \right) \tag{10}$$

2.5.3 Modeling Vegetation Water Potential

The PHS model within CLM5 uses Darcy's law to model the flow of water through the SPAC, which can be represented with an electrical circuit analogy (Figure 1). PHS solves for vegetation water potential along the path from soil-to-atmosphere. Vegetation water supply (root water uptake) and demand (transpiration) are both coupled to vegetation water potential, such that the solution for vegetation water potential is the set of values that matches supply with demand.
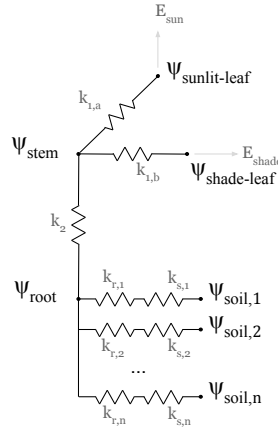
Figure 1. Plant hydraulic circuit analog schematic

PHS solves for vegetation water potential at four locations: ψ_{root}, ψ_{stem}, $\psi_{\text{shade-leaf}}$, and $\psi_{\text{sun-leaf}}$. The number of nodes is chosen as the strict minimum to allow for differences in segment parameterizations [*Simonin et al.*, 2015; *Sperry and Love*, 2015], while also conforming to existing CLM model structure (vertically discretized soil layers, 2-big-leaf). At each node in the circuit diagram in Figure 1 we model water potential, and, between nodes, we resolve the flux of water based on Darcy's law. Water uptake from the different soil layers is assumed to operate in parallel; a typical assumption justified by higher resistance in lateral versus central roots (e.g. *Williams et al.* [2001]). Two resistors operate in series between each ψ_{soil} and ψ_{root}, to represent the path across the soil matrix and then through the root tissue [*Williams et al.*, 1996]. Specifics on the parameterization of hydraulic conductance for each segment are provided in Appendix B.1.

2.5.4 PHS solution

PHS solves for the set of vegetation water potential values (ψ) that matches water supply (root water uptake) to water demand (transpiration), while satisfying continuity across the four water flow segments (soil-to-root, root-to-stem, stem-to-leaf, and leaves-to-transpiration). Beginning from an initial condition of ψ (from the previous timestep), PHS computes the

flux divergence f (representing the mismatch of flow in and out of each segment) and iteratively updates ψ until it reaches convergence, i.e. $f \to 0$.

$$\psi = \begin{bmatrix} \psi_{\text{sun}} \\ \psi_{\text{shade}} \\ \psi_{\text{stem}} \\ \psi_{\text{root}} \end{bmatrix} \tag{11}$$

$$f(\psi) = \begin{bmatrix} E_{sun} - q_{sun} \\ E_{shade} - q_{shade} \\ q_{sun} + q_{shade} - q_{stem} \\ q_{stem} - \sum_{j=1}^{n} q_{root,j} \end{bmatrix} \tag{12}$$

$$A = \frac{df}{d\psi} \tag{13}$$

While $|f| > 0$

$$\Delta\psi = A^{-1} f(\psi_i)$$
$$\psi_{i+1} = \psi_i + \Delta\psi \tag{14}$$

The numerics are tractable because f has continuous, analytical derivatives and A (a 4x4 matrix with six null entries) is easy to invert when well-conditioned. Supply and demand converge, because transpiration demand decreases with more negative leaf water potentials and supply increases with more negative leaf water potentials. The PHS loop is nested within iterations for intercellular CO_2 concentration and leaf temperature. As described earlier, within a set of PHS iterations (14), transpiration is assumed to be linear with f_w. The non-linear relationship between f_w and transpiration is resolved through iteration for converging f_w alongside intercellular CO_2. Details on the numerical implementation are provided in Appendix Section B.1.

2.5.5 Water supply

Water supply is modeled via Darcy's Law, where flux of water (q) is the product of the path hydraulic conductance (k) and the gradient in water potential ($\psi_2 - \psi_1$) after accounting for gravitational potential ($\rho g \Delta z$). Equation 15 represents the flow from a generic node 1 to node 2.

$$q = -k(\psi_2 - \psi_1 + \rho g \Delta z) \tag{15}$$

For simplicity, PHS does not represent plant tissue water storage (or capacitance, using the electrical circuit analogy), and is in line with recent supply-loss theory [*Sperry and Love*, 2015]. Capacitance significantly complicates the water potential solution [*Celia et al.*, 1990] and is challenging to parameterize [*Bartlett et al.*, 2016]. However, buffering of water stress provided by tissue water storage could potentially be important especially on sub-daily timescales [*Meinzer et al.*, 2009; *Epila et al.*, 2017], whereby its inclusion may be warranted in future model versions.

Hydraulic conductance through vegetation segments is modeled following empirical xylem vulnerability curves [*Tyree and Sperry*, 1989], where segments lose conductance with increasing xylem tension related to cavitation and embolism [*Holbrook et al.*, 2001]. The vulnerability curves model loss of conductance relative to maximum conductance (k_{max}) using two parameters: c_k, a sigmoidal shape-fitting parameter, and p_{50}, the water potential at 50% loss of segment conductance (following *Gentine et al.* [2016]).

$$k = k_{\max} 2^{-\left(\frac{\psi_1}{p_{50}}\right)^{c_k}}$$ (16)

Both c_k and p_{50} can be estimated from field experiments [*Sack et al.*, 2002], and p_{50} is available in the TRY trait database [*Kattge et al.*, 2011]. Parameterization based on p_{50} aligns with the call for a transition to models that use a wider range of plant functional trait data in their parameterization [*Anderegg*, 2015a]. The loss of xylem conductivity is based on lower terminal water potential (ψ_1) as is typical in other simplified models [*Xu et al.*, 2016], but may underestimate the integrated loss of conductivity [*Sperry and Love*, 2015].

PHS models root, stem, and leaf tissue conductances according to equation 16. The parameterization of $k_{\max}$ varies by hydraulic segment (see details in Appendix B1). The conductance across the soil matrix to the root surface follows *Williams et al.* [2001] and *Bonan et al.* [2014]. Bulk soil resistivity is based on *Clapp and Hornberger* [1978] as described in *Oleson et al.* [2013]. Details are provided in Appendix B1.

2.5.6 Water demand

Water demand is calculated using the Medlyn stomatal conductance model (see Section 2.1) modulated by the CLM water stress factor. As discussed earlier f_w is based on leaf water potential in PHS, where stress increases as leaf water potential becomes more negative [*Klein and Niu*, 2014]. Because leaf water potential is modeled separately for sunlit and shaded leaves, f_w takes on distinct sunlit and shaded values.

$$f_{w,sun} = 2^{-\left(\frac{\psi_{\text{sun-leaf}}}{\psi_{50}}\right)^{c_k}}$$
$$f_{w,shade} = 2^{-\left(\frac{\psi_{\text{shade-leaf}}}{\psi_{50}}\right)^{c_k}}$$ (17)

Shaded and sunlit leaf transpiration (E_{sun}, E_{shade}) are calculated by attenuating maximal transpiration ($E_{\text{sun,max}}$, $E_{\text{shade,max}}$) according to f_w. $E_{\text{sun,max}}$ and $E_{\text{shade,max}}$ are calculated at the beginning of each timestep by running the stomatal conductance model with $f_w = 1$. Equations (17) and (18) reflect a simplification used within iterations of the PHS module, neglecting non-linear components of the relationship between stress and transpiration (described further in Section zqz).

$$E_{\text{sun}} = f_w E_{\text{sun,max}}$$
$$E_{\text{shade}} = f_w E_{\text{shade,max}}$$ (18)

3 Experiment Description

We use a set of four simulations to assess the impact of the plant hydrodynamics model (PHS versus SMS) on a throughfall exclusion experiment.

1. SMS, with ambient precipitation throughfall (AMB)
2. SMS, with 60% of precipitation throughfall excluded (TFE)
3. PHS, AMB
4. PHS, TFE

All four simulations use the same version of CLM5 (development version r270, www.github.com/ESCOMP/ctsm/releases/t which features a switch that can toggle between SMS and PHS configurations. Simulations are run offline (uncoupled from an active atmospheric model), spanning from 2001 through 2003, utilizing the satellite phenology (SP) mode of CLM5 in which vegetation state (LAI,

Table 1. Select parameter values

CLM name	Full Name	Symbol	Value
kmax(1)	Maximum Sun Branch Conductance	$k_{1a,\mathrm{max}}$	4e-8 s^{-1}
kmax(2)	Maximum Shade Branch Conductance	$k_{1b,\mathrm{max}}$	4e-8 s^{-1}
kmax(3)	Maximum Stem Conductivity	$k_{2,\mathrm{max}}$	4e-8 m/s
krmax	Maximum Root Conductivity	$k_{r,\mathrm{max}}$	6e-9 m/s
psi50	Water potential at 50% loss of conductivity	ψ_{50}	-1.75 MPa
ck	Vulnerability shape parameter	c_k	2.95
smpso	Soil potential with stomata fully open	ψ_o	-0.65 MPa
smpsc	Soil potential with stomata fully closed	ψ_c	-2.5 MPa
medlyn_intercept	Medlyn intercept	g_0	100 μmol / m2 / s
medlyn_slope	Medlyn slope	g_1	6 kPa$^{0.5}$
n	Soil porosity to 4.64 meters	n	0.42
n	Soil porosity beyond 4.64 meters	n	0.28
hksat	Saturated soil hydraulic conductivity	$k_{s,\mathrm{max}}$	3e-5 m/s
sucsat	Saturated soil matric potential	ψ_{sat}	461 Pa
bsw	Brooks-Corey parameter	b	6

canopy height) is prescribed and biogeochemistry is inactive. Six-year spin-up simulations (one each for SMS and PHS) are used to create initial conditions, repeating the Ambient simulation twice. Descriptions of site characteristics, forcing data, and observational sap flux and soil moisture, can be found in *Fisher et al.* [2007] and *Fisher et al.* [2008].

3.1 Parameter Values and Throughfall Exclusion

Parameter values concerning vegetation hydrodynamics are presented in Table 1. All other parameters use the default values associated with the r270 version of CLM5. Informed by parameter values reported in *Fisher et al.* [2008], we tuned soil hydraulic parameters and throughfall exclusion rates to be in the range of observed soil moisture (Supp Fig A.9). A 972-member ensemble of simulations was used to tune the parameters for the PHS configuration to reasonably reflect sap flux observations (see Appendix B.4). No tuning was used for the SMS configuration.
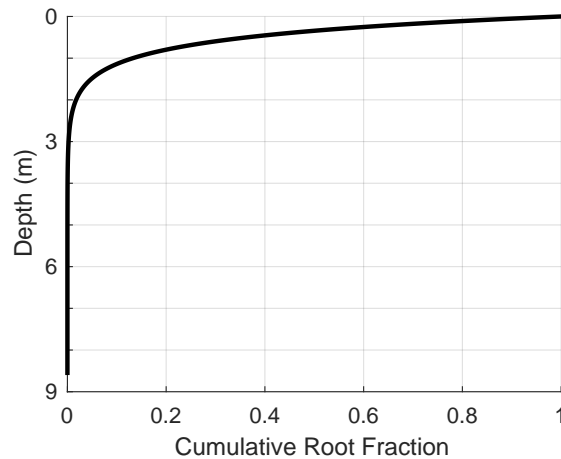
Figure 2. Cumulative rooting distribution

4 Results

4.1 Comparison with observations

We tested two configurations of CLM5 with simulations of the Caxiuanã throughfall exclusion experiment over 2002-2004. We compare modeled transpiration with observations derived from sap flux velocity and modeled soil moisture with observations using TDR sensors (see Section 3 for experiment and observation details).

4.1.1 Transpiration, Ambient Conditions

Under ambient conditions, PHS reduces error and improves correlation between modeled and observed transpiration (compared to SMS, Figure 3a,c). While the two models make a similar number of small errors (PHS/SMS model transpiration within 0.15 mm/d of observations in 106/94 of the 414 days with available observations), SMS commits more large errors. The absolute value of SMS-OBS (Figure 4g) exceeds 1 mm/d in 67 times, as compared to just 23 with PHS. And while PHS error is limited to a maximum of 1.6 mm/d, SMS error exceeds 2 mm/d twelve times (all of which underestimate transpiration relative to observations).

Notwithstanding improvements regarding RMSE and correlation, the PHS simulation seems to underestimate transpiration variability, with a standard deviation of 0.61 mm/d compared to 0.87 mm/d in the observations (with SMS, the standard deviation is 0.97 mm/d). As such, PHS features a low bias for high transpiration values and a high bias for low transpiration values (Figure 3c). The difference in modeled transpiration between PHS and SMS derives from divergent water stress dynamics, which are presented in Section zqz.

4.1.2 Transpiration, TFE

Both models have a harder time modeling transpiration under TFE, with higher RMSE and lower correlation compared to the ambient simulations (Figure 3b,d). PHS improves on SMS, with lower RMSE and higher correlation, but with a significant high bias (Figure 3b,d). Observations show a 41% reduction in transpiration due to TFE, as compared to a 21% reduction in modeled transpiration with PHS (and 32% with SMS). The PHS bias seems to decrease over time (Figure 4), suggesting that the model may lag in its response to the TFE. Reproducing the effect of TFE has precedent in the literature, and has not been captured well by the CLM (nor other DGVMs) [*Restrepo-Coupe et al.*, 2017; *Powell et al.*, 2013].

4.1.3 Soil Moisture

The second source of observations for model evaluation are volumetric soil moisture. These are valuable, because the parameterization of root water uptake is updated with PHS. Modeled soil moisture values (at a depth of 50 cm) are comparable during the wet season (February-March-April) under ambient conditions, both yielding averages of 28% (Figure 5a,c). Under these conditions (excess rainfall), soil moisture is largely determined by the soil field capacity. With water shortfalls, the root water uptake parameterizations drive the soil moisture dynamics, and the models diverge, with SMS consistently generating lower soil moisture values (than PHS) within the first meter of the soil column (Figure 5, Supp Fig A.10). Soil moisture averages to 10% during the dry season (September-October-November, ambient case, depth=50cm) with SMS, as compared to 16% with PHS. PHS better comports with observations, reducing RMSE by 57% relative to SMS (Figure 5a,c).

Under TFE, SMS minimum soil moisture is again limited to 10%, but holds there for a longer duration (Figure 5). Contrastingly, PHS achieves lower dry season soil moisture values under TFE. Again PHS better comports with observations, reducing RMSE by 42% relative to SMS (Figure 5a,c). We highlight the soil moisture at 50 cm depth, but similar patterns

are observed throughout the first meter of the soil column (Supp Fig A.10). To emphasize the effect of root water uptake, we opt for the depth of 50 cm, because it features higher root fraction than the deeper soil layers, but avoids the high frequency dynamics of the top soil layer from soil evaporation and precipitation events.

4.2 Vegetation water potential

PHS updates both the water stress and root water uptake parameterizations based on modeling vegetation water potential. Leaf water potential shows typical diurnal drop, reaching -1.65 MPa at midday (Figure 6a). Most of the midday pressure drop occurs between ψ_{root} and ψ_{stem} (Δ=-1.47 MPa), representing the root collar and upper stem, respectively. Stem shade and leaf are all identical.

Under TFE, model midday leaf water potential decreases to -2.31 MPa (Figure 6b). This change derives from a decrease in predawn root water potential (lower soil moisture) and an increase in the drop in root water potential between predawn and midday (due to reduced soil-to-root conductance). This comports with previous evidence that seasonal changes in hydraulic resistance are larger belowground [*Fisher et al.*, 2006]. Despite reduced stem conductance, the pressure drop from root-to-stem actually decreases to -1.02 MPa, with transpiration reduced by 54%. In this way, stomatal regulation serves to mitigate the drop in leaf water potential due to soil drying and reduced hydraulic conductance.

Midday leaf water potential features seasonal cycle, with lower values during the dry season. Under ambient conditions, modeled root water potential values match wet season observations, but are less negative than dry season observations [*Fisher et al.*, 2006]. Modeled leaf water potential values under ambient conditions are less negative than field observations (*Fisher et al.* [2006] report average ψ_{leaf} of -1.71 MPa during the wet season and -2.47 MPa during the dry season), but are within the range of observations. The parameter values used here may underestimate isohydricity (which would be reflected by minimal leaf water potential drop during drought) in response to TFE, showing a significant drop in leaf water potential of 0.66MPa (dry season, 2003), whereas observations showed no significant difference [*Fisher et al.*, 2006].

4.3 Stress factor

Modeling vegetation water potential enables a diurnal mode of variability in vegetation water stress. While the SMS stress factor has minimal diurnal variability (Figure 7a), PHS features increased stress at midday (Figure 7b), corresponding to the drop in leaf water potential (Figure 6b,c). While average midday stress values are comparable during the 2003 dry season (Figure 7) between the two model configurations, PHS achieves more photosynthesis (Supp Fig A.2), due to the lower stress in the mornings and afternoons.

Indeed, the PHS stress factor responds to both soil moisture and VPD (Figure 8c,d), while SMS responds only to soil moisture (Figure 8a,b). This dependence on VPD results in more wet season stress with PHS (as compared to SMS) under both ambient and TFE conditions (Figure 9a-d).

4.4 GPP

The two models predict similar GPP during the TFE simulation (2002-2003), with 1.98 kgC/m^2/yr for SMS and 2.00 kgC/m^2/yr for PHS, but GPP is lower for PHS under ambient conditions (2.43 kgC/m^2/yr) as compared to SMS (2.73 kgC/m^2/yr, Figure 9e-h). Seasonal variability in GPP is smaller with PHS, especially under ambient conditions. The standard deviations of daily GPP (2002-2003) are 0.49 and 1.55 gC/m2/d for AMB/TFE, as compared to 1.53, 2.73 gC/m2/d with SMS. Lower maximal photosynthesis and less variability in GPP are both related to updates to the water stress factor implemented with PHS.

Table 2. Root-zone soil potential ^{a} (MPa) terciles for Figure 8

Simulation	T1	T2
SMS, Ambient	-0.01	-0.54
SMS, TFE	-0.29	-1.74
PHS, Ambient	-0.01	-0.05
PHS, TFE	-0.05	-0.33

^{a}SMS values correspond to daily mean root-fraction weighted soil potential. PHS values correspond to predawn root water potential.

PHS has a stress response to high levels of transpiration (Supp Fig A.5c,d) due to the associated drops in leaf water potential. This negative feedback limits maximal transpiration and photosyntheis, while reducing variability. Transpiration shows a seasonal pattern in both models (Figure 3a,b), but with a larger amplitude for SMS. For example, under ambient conditions, the 10th and 90th percentiles for daily total transpiration with SMS are 1.65 and 4.22 mm/d (Δ=2.57 mm/d). That range exceeds the span for PHS: 1.85 and 3.49 mm/d (Δ=1.64 mm/d). Under ambient conditions, PHS underestimates transpiration variability as compared to sap flux observations (Figure 3e). However PHS yields a better overall fit to the field observations, with higher R^2 and lower RMSE compared to SMS under both ambient and TFE conditions (Figure 3c-f, Table 3).

Table 3. Summary statistics evaluating the relationship between modeled transpiration and sap flux observations (plotted in Figure 3)

Simulation	R^2	RMSE (mm/d)
SMS, Ambient	0.434	0.764
PHS, Ambient	0.742	0.508
SMS, TFE	0.303	1.026
PHS, TFE	0.449	0.741

4.5 Root water uptake: dynamics

Root water uptake is more sensitive to soil potential with PHS (Figure 12), which follows from sharp declines in hydraulic conductance with drying. Hydraulic conductance decreases by approximately three orders of magnitude across the range of PHS soil potential (Supp Figure A.6b). In contrast, the SMS-implied conductance increases with drying over most of the soil potential domain, until ψ_{soil} reaches -2.5MPa, beyond which it is defined to equal 0 (Supp Figure A.6a). Root water uptake still decreases with SMS as soils dry beyond -2.5MPa, but only because of the decrease in $\Delta\psi$ (Supp Figure A.7c). Whereas PHS imparts a diurnal cycle to root water uptake via dynamic root water potential, the hydraulic gradient with SMS is defined by ψ_c, which is constant, requiring a diurnal cycle in the (implied) hydraulic conductance (Supp Figure A.7).

4.6 Root water uptake: profiles

Overall, the two model configurations feature comparable transpiration during the dry season under ambient conditions (PHS: 28.3cm, SMS: 28.5cm). However they feature distinct vertical profiles, as PHS removes less water from intermediate soil layers (0.5-1.5meters) (Figure 11d). SMS removes more water from these layers, due to the lower sensitivity of root

water uptake to soil potential. Likewise, partitioning of root water uptake within the soil column is more sensitive to precipitation in PHS (Figure 11a-c). In PHS, during the longer periods without rain, surface extraction plateaus and transpiration is fueled by the deeper soil water. After rain events, surface extraction renews, while at depth, root water fluxes reverse, with water deposited through root hydraulic redistribution instead of being extracted. Both models decrease surface extraction under TFE (Figure 11b), but PHS has a larger compensation from below 0.2m (Figure 11c), allowing more overall transpiration (14.6 vs. 10.8 cm).

During the wet season PHS utilizes more water from the near-surface soil layers (Figure A.3b), with zero net root water uptake below soil depth of 35.2 cm in ambient conditions (or beyond 9.6cm under TFE). SMS extracts 49.8% (AMB) and 81.5% (TFE) of total transpiration from beyond those levels (Figure A.3). PHS does extract some water from beyond 35.2/9.6cm into the soil profile, but in service of hydraulic redistribution, sending the extracted water deeper into the soil column.

4.7 Hydraulic redistribution

SMS precludes hydraulic redistribution (HR) setting root water uptake to zero when reversed gradients in water potential occur (contrary to PHS). With PHS, HR totals to 38.9 cm under ambient conditions and 40.0 cm under TFE over the course of 2003, with the majority (28.0, 26.7 cm) of this HR occurring at night (Figure 10). HR occurs in both directions (Supp Fig A.8), but is predominately downwards (AMB: 30.7cm, TFE: 33.8cm). Likewise HR occurs during both the wet and dry seasons. The seasonality changes with TFE, as AMB has more HR during Sept-Jan, while TFE features more HR during Feb-Apr.

4.8 Soil moisture effect on transpiration

Model soil potential shows limited relationship to sap flux observations under ambient conditions (Supp Fig A.11b,f), which is indicative of limited soil moisture stress. However, in the SMS configuration, modeled transpiration decreases strongly with more negative soil potential (Supp Fig A.11a), biasing the model relative to observations (Fig 14a).

Sap flux observations under TFE show a stronger relationship with soil potential especially with PHS (Supp Fig A.11h,d). With SMS, the modeled attenuation of transpiration with soil potential again seems to bias modeled transpiration (Fig 14b). Derived from ψ_c, transpiration approaches zero when soil potential reaches -2.5 MPa (Supp Fig A.11c). The two PHS simulations feature less structure in transpiration bias vs. soil potential and less bias overall (Fig 14c,d).

5 Discussion

5.1 Can modeling vegetation water potential improve the CLM?

In this study, we have implemented plant hydraulic theory within CLM5, using dynamic vegetation water potential to modulate leaf gas exchange and root water uptake. PHS installs a model for predicting vegetation water potential by extending Darcy's Law through the vegetation substrate (Figure 1), creating four new water potential prognostic variables (ψ_{root}, ψ_{stem}, $\psi_{shade-leaf}$, and $\psi_{sun-leaf}$). The model is able to capture expected diurnal and seasonal dynamics of vegetation water potential, with lower values within the stem and leaves at midday and during the dry season (Figure 6).

Beyond matching observations of leaf and stem water potentials, the ambition of plant hydraulic models is to advance the physical basis for modeling the SPAC, while improving predictions of water and carbon fluxes. Following from this, the bulk of our analysis and discussion pertains to how modeling vegetation water potential can be used to improve the

representations of transpiration, root water uptake, and soil moisture dynamics within the CLM.

5.2 Water stress and stomatal conductance

PHS uses leaf water potential as the input to the water stress factor, replacing the previous version based on soil water potential (SMS). Using leaf water potential permits a representation of xylem tension stress and its diurnal variations, where vegetation must limit transpiration to avoid cavitation and embolism. This limitation is in addition to the VPD response of the Medlyn stomatal conductance model, which optimizes carbon gain versus water losses [*Medlyn et al.*, 2011]. Opting for xylem tension stress (PHS), in lieu of soil moisture stress (SMS), inserts an alternative physical interpretation of water stress and also yields different stress dynamics, which has significant support in the literature [*Novick et al.*, 2016b; *Sperry et al.*, 2017].

Basing stress on leaf water potential imparts a diurnal cycle to the water stress factor (Figure 7), following the midday drop in leaf water potential induced by high leaf-level VPD and photosynthesis. As such, water stress now depends on transpiration demand, and, in turn, leaf-level VPD and radiation (Figure 8, Supp Fig A.4) and not only on soil moisture stress. The PHS water stress factor also exhibits a seasonal cycle, with lower values (indicating more stress) during the dry season. However, the seasonal variation in water stress is smaller than with the control model (Figure 9a-d).

As a result, PHS (compared to SMS) features less seasonal variability in GPP and transpiration, especially under ambient conditions (Figures 9e-h, 3a,c). Furthermore, PHS exhibits less variability in transpiration than observations derived from sap flux velocity (Figure 3e,f). This follows from a negative feedback on GPP induced by the PHS water stress factor. Conditions favoring increased GPP (e.g. more light) also increase xylem tension and stress, which opposes increases in GPP. This negative feedback could be loosened by adjusting parameters to increase the hydraulic safety margin, such as increasing maximum stem hydraulic conductance. *Restrepo-Coupe et al.* [2017] show that GPP at Caxiuanã is highest during the dry season, suggesting that both models fail to capture the observed GPP seasonal cycle.

Likewise, both models produce a high bias in transpiration under TFE (Figure 3a,b). A previous study testing the CLM (version 3.5) with the Caxiuanã TFE experiment also found that the model underestimated the effect of the drought treatment [*Powell et al.*, 2013]. This might suggest model structural or parametrics deficiencies that are external to the water stress parameterization.

Overall, PHS provides a better match to sap flux observations, featuring lower RMSE and higher correlation, especially under ambient conditions. This result should be tempered by the fact that model tuning was not symmetrical between the two configurations (see Section 3). However, in Section 5.5, we discuss further evidence that suggests that PHS provides significant improvements in modeling water stress and its effect on transpiration.

5.3 Structural improvements in modeling root water uptake

In addition to modulating water stress and transpiration, vegetation water potential can be used to improve the CLM representation of root water uptake. PHS uses dynamic root water potential (ψ_{root}, Figure 6) as the sink for measuring the hydraulic gradient governing root water uptake ($\Delta\psi$). Because SMS does not resolve water potential through the vegetation substrate, the model instead uses a constant parameter, ψ_c, in its definition of $\Delta\psi$. As such, PHS provides a critical structural improvement for modeling root water uptake, consistent with extensive evidence of dynamic vegetation water potential (e.g. *Fisher et al.* [2006]).

Root water uptake dynamics are driven by either changes in $\Delta\psi$, as discussed above, or by changes in hydraulic conductance, k. PHS features mechanistic reductions in k based on root xylem vulnerability and soil hydraulic properties, conforming to soil-root hydraulic theory [*Cai et al.*, 2014; *Warren et al.*, 2015]. As a result the soil-root conductance features a strong, positive relationship with soil potential, decreasing by almost three orders of magnitude as the soil dries (Supp Fig A.6). Hydraulic conductance is not explicitly modeled with SMS, but the values implied by the transpiration partitioning function (see Section 2.4.2), actually increase as soils dry over the domain of $\psi_c < \psi_{\text{soil}} < \psi_o$ (Supp Fig A.6).

Furthermore, whereas SMS uses a relative notion to scale uptake by root abundance (root fraction), PHS opts for an absolute measure (root area), which can better capture dynamic carbon allocation in response to drying. With SMS, if root mass were to double in every soil layer, the root fraction remains unchanged, yielding no advantage in accessing soil water. With PHS, as root area in a soil layer increases so does the hydraulic conductance, even if the layer root fraction remains constant.

PHS appropriately penalizes extraction of soil water from deep in the soil column, associated with increased distance between roots, increased xylem length, and contributions from gravity (all factors not represented in SMS). As a result, PHS favors surface extraction when water is available (Figure A.3). The model can overcome these penalties, featuring compensatory root water uptake where extraction (during the dry season) from beyond 2-meter depth increases significantly in response to TFE (Figure 11). Dynamic root potential (and conductance) gives PHS more flexibility, allowing the model to switch root water uptake to the lower layers as the surface dries out.

Finally, PHS eschews the unsubstantiated constraints on $\Delta\psi$ imposed by SMS ($0 \geq \Delta\psi \geq \psi_c - \psi_o$, see Section 2.4.1). Allowing $\Delta\psi$ to change sign yields a representation of hydraulic redistribution, which has been observed in Amazonian forests [*Oliveira et al.*, 2005].

5.4 Hydraulic Redistribution (HR)

Substantial HR is simulated at our test site, both upwards and downwards (Figure 10, Supp Fig A.8), as has been observed in the field [*Burgess et al.*, 1998]. Modeled HR is dominated by downward transfers, moving near-surface water from rain events deeper into the soil column and thus saving it for when it is most needed such as during the dry season. This would seem to convey an advantage to deep-rooted individuals, banking water for later use out of reach of shallow-rooted competitors. HR can offer significant water subsidies during dry periods [*Jackson et al.*, 2000] and has been highlighted as an important missing feature in CLM [*Lee et al.*, 2005]. We should note that observations of HR are extremely difficult and rare, and the degree to which HR actually occurs in real-world systems remains unclear. Unequivocal detection of HR involves the observation of reverse flow along transport roots, typically at rates close to the detection threshold of sap flow monitoring systems.

One challenge we faced was that in an initial implementation of PHS, HR seemed to oversupply the top layer of the soil column (spanning 0 to 2 cm below the ground surface) and thus significantly degraded modeled soil evaporation (not shown). To remedy this problem, we set the hydraulic conductance to zero in the uppermost soil layer, disallowing any root water uptake there.

In our simulations, HR increases root water uptake by up to 52% relative to transpiration alone (2003, TFE).

PHS naturally represents HR, as it follows directly from Darcy's Law, occurring when water potential in a given soil layer is more negative than ψ_{root}. However, it remains to be seen whether HR, as modeled in this implementation, is a feature or a liability. PHS may overestimate HR, given the simplified root system architecture [*Bouda and Saiers*, 2017] and

the lack of an explicit representation of fine-root cavitation [*Kotowska et al.*, 2015]. Other models, similar to the SMS paradigm, disallow HR by constraining root water uptake to be positive [*Xu et al.*, 2016]. We view this first implementation of HR into the default versions of the CLM as a 'null' hypothesis for the functioning of this process, and as a platform to allow further refinement from the plant hydraulics community. Isotopologues of water could be used as a tool to further constrain this redistribution in CLM in the future.

5.5 Soil moisture dynamics

Partly due to HR, vertical and temporal gradients in soil water potential are significantly reduced in PHS (Figure 13). This can also be attributed to the root water extraction hydraulic gradient ($\Delta\psi$), which is significantly smaller in PHS (Supp Fig A.7). In turn, SMS features a significant dry bias relative to soil moisture observations, especially in the first meter of the soil column. This indicates that SMS root water uptake is 'pulling' too hard, and that ψ_c is too low, at least regarding soil moisture dynamics. PHS reduces soil moisture RMSE by up to 55% relative to SMS (Figure 13).

In the literature, ψ_c is primarily associated with its role governing the response of transpiration and photosynthesis to soil moisture [*Powell et al.*, 2013; *Bonan et al.*, 2014; *Rogers et al.*, 2017]. We show that it likewise has significant control over soil moisture, itself. Throughout the four simulations, ψ_c (equals -2.5MPa) is significantly lower than ψ_{root}, yielding a larger hydraulic gradient, and the dry bias in soil moisture. Likewise, during dry periods, soil potential has a tendency to take on the specific value of ψ_c over significant areas of space/time. Constrained to the top 2 meters of the soil column (which contains 98% of the total root fraction, Figure 2), 38.9% of the space-time area in Figure 13a is within 0.1 MPa of ψ_c. This can occur even without TFE, where Soil Layer 8 (spanning 68 to 92cm below ground) spends 23.2% of the time during 2003 within 0.1 MPa of ψ_c (Supp Fig A.9a) under ambient conditions. Through its effect on root water uptake (Equation 7) ψ_c serves as an effective minimum soil water potential (outside of layers influenced by soil evaporation). In addition, due to the discontinuity of the root water uptake equation that occurs at ψ_c, soil water potential has a tendency to trend towards and then stick at ψ_c during dry periods. PHS instead adopts a more physical model for root water uptake (Equation 10) that avoids this discontinuity, preserves some soil moisture variability during dry periods (Figure 13), and better conforms to hydraulic theory.

5.6 The influence of soil moisture on transpiration

The stress effects of declining soil water potential seems to bias SMS predictions of transpiration relative to sap flux observations (Figure 14a,b). Under ambient conditions, soil water shows little relationship with sap flux observations with either model configuration (Supp Figure A.11b,f), however SMS modeled transpiration decreases strongly in response to soil drying (Supp Figure A.11a). This creates a bias where SMS underestimates transpiration during the drier soil conditions, which is in line with *Bonan et al.* [2014], where the water stress factor was found to impose too much attenuation of transpiration (in CLM4.5). With PHS the transpiration bias does not seem to strongly depend on soil potential, while also featuring less bias overall (Figure 14c,d). Likewise PHS yields a stronger relationship than SMS between soil potential and sap flux observations during TFE (Figure A.11d,h). This could indicate that PHS better models the relationship between soil potential and water stress and/or the soil moisture dynamics itself. The reduction in bias introduced by the water stress function (especially as it depends on soil potential) represents a major development, given repeated calls to improve vegetation water stress in the next generation of terrestrial biosphere models [*Powell et al.*, 2013; *Rogers et al.*, 2017].

5.7 Benefits and limitations of PHS

5.7.1 Benefits

1. parameters are better represented in trait database
2. creates an interface to VOD data
3. platform for testing various hydraulics hypotheses
   - xylem tension and/or hydraulic cost limitation to g_s
   - drought-informed dynamic allocation
4. improved soil moisture and transpiration dynamics (subject to asymmetrical tuning)
5. advanced physical realism for RWU
   - reflects dynamic veg water potenial
   - responds to absolute measure of root biomass
   - eschews constraints that on one side preclude HR and the other set an effective minimum ψ_{soil}

5.7.2 Limitations

1. hydraulics are simplified
   - no capacitance
   - vulnerability not integrated across veg tissue or soil matrix
   - stem-to-leaf resistance is not fully deployed
   - simplified root system architecture
   - but the simplifications do add up to a nice null hypothesis for further testing and yield a relatively light-weight model
2. uncertainty regarding the application of water stress
   - we apply to V_{cmax}
3. more parameters
4. scale mismatch to reported parameter values in trait database
   - likewise does not necessarily comport well with PFT paradigm
5. we don't provide a definitive assessment on model skill
   - asymmetrical model tuning
   - especially when taking into account the increased number of parameters
   - however PHS offers better alignment with established theory and shows promising result in removing bias introduced by the water stress factor

6 Conclusion

The PHS configuration of the CLM5 within the Community Earth System Model (CESM)is, to our knowledge, the first land-surface model within an ESM with a representation of plant water potential running in its default configuration. In this paper, we have described the model implementation, and illustrated a comparison of the model dynamics for a tropical rainforest site subjected to water limitation, given that prediction of rainforest responses to drought is one of the key uncertainties in the ESM predictions [*Huntingford et al.*, 2013]. Overall, the new model behaviour differs from the default configuration in ways that are expected, given its structural properties, and in many cases, provides better correspondence with observations than the default structure.

In this paper, however, we did not aimed at undertaking a comprehensive assessment of which model structure performs better, given the substantial parametric uncertainty in both

models, and the dependence on numerous other features of the CLM external to water stress representation that contribute to model-observation divergences - in this case in particular, the overestimation of unstressed transpiration by both versions of the model compared to the observations.

In lieu of this type of assessment, we propose that the new PHS model structure 1) is more closely aligned with known plant hydraulics theory, 2) provides significantly improved connections to real-world observational data streams (of leaf and stem water status, sap flow, percent loss conductance) and 3) represents known features of ecohydrological function that the default model cannot capture, including hydraulic redistribution, changes in the depth of water uptake with drought stress, plant embolism impacts on gas exchange and responses of water uptake to changes in leaf:root ratios.

7 Cut from other sections

Plant hydraulics can potentially improve model predictions of vegetation response to climate change [*Sperry and Love*, 2015], especially if parameter ranges and model complexity can be constrained [*Rogers et al.*, 2017]. Numerous site-level models have deployed plant hydraulics (e.g. *Williams et al.* [1996]; *Sperry et al.* [1998]; *Bohrer et al.* [2005]), and studies show vegetation water potential can improve predictions of stomatal response to the environment [*Sperry et al.*, 2017; *Anderegg et al.*, 2017], More recently hydraulics have been coupled to global models [*Bonan et al.*, 2014; *Xu et al.*, 2016; *Christoffersen et al.*, 2016], but most Earth System Models do not provide a mechanistic representation of vegetation water dynamics.

Incorporating hydraulic theory into Earth System Models is a well established ambition in the field of ecohydrology [*Sperry and Love*, 2015], supported by potential improvements in modeling mortality and productivity [*Choat et al.*, 2012; *McDowell et al.*, 2018]. However, concerns exist in the literature regarding hydraulic model complexity and parameterization [*Verhoef and Egea*, 2014; *Drake et al.*, 2017], which led to a series of simplifications implemented in our model design (see Section 2). Recent work suggests model complexity can be managed, given the significant coordination of hydraulic traits [*Bartlett et al.*, 2016; *Christoffersen et al.*, 2016]. Furthermore incorporating plant hydraulics provides access to new streams of observational data for model validation and parameterization. Vegetation water potential can be monitored in the field [*Boyer*, 1967] and has been shown to correlate with microwave remote sensing products [*Momen et al.*, 2017]. Parameter values can be measured in the field [*Sack et al.*, 2002] and are available in the TRY database [*Kattge et al.*, 2011].

Modeling stomatal conductance and photosynthesis, especially subject to water stress, is an area of ongoing research. We use the Medlyn VPD-dependence model coupled to a hydraulic stress function that attenuates V_{cmax}. This complies with observations [*Lin et al.*, 2018; *Zhou et al.*, 2013] that stress applied through g_1 underestimates attenuation of photosynthesis. However, there is no direct evidence of declines in V_{cmax} at the leaf level with drought [*Flexas et al.*, 2006], whereby future work may seek to represent mesophyll conductance in CLM to correct such discrepancy.

The model hydraulic supply representation is simplified, to reduce the model parameter and computational burdens. No capacitance. No integration of xylem or soil conductances vulnerability, instead based on lower node. No hysteresis in loss of conductance, xylem instantly regain conductance upon re-wetting. Leaf conductance simplified. Soil layers fully parallel, soil potential constant each time step.

Parameter uncertainty is significant. Notions of hydraulic architecture will never perfectly fit on this modeling scale, especially in a PFT paradigm. Field measurements of hydraulic traits will help constrain parameter ranges, but mostly only aboveground. Flux observations can help to tune stress parameters. Parameter estimation for root functioning is

740 significantly more challenging, given the difficulty in underground trait observations. Like-
741 wise observational constraints of vertically-resolved states and fluxes underground are scarce.
742 Follow-up work will be geared towards parameter estimation and assessing model skill.

743 Partitioned among the segments of the SPAC, the changes in leaf water potential (to-
744 taling -0.66MPa) due to TFE are: -0.44MPa soil potential, -0.66MPa soil-to-root, +0.45MPa
745 root-to-stem, and -0.001MPa stem-to-leaf.

746 **8 Acknowledgments**

747 **9 Figures**
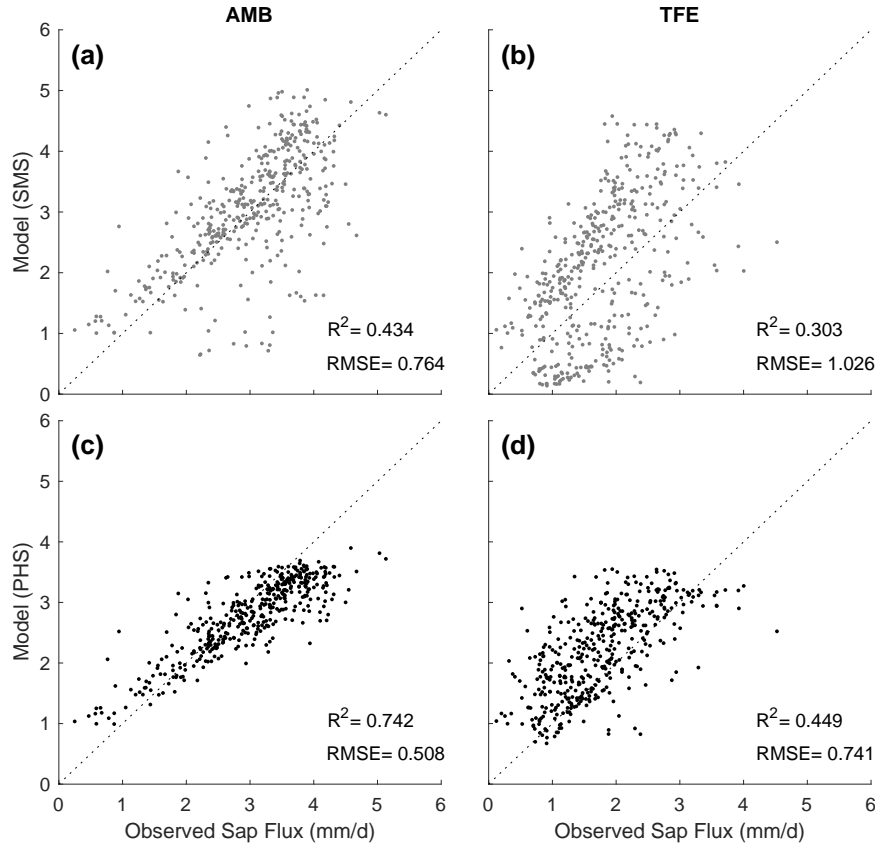
748 **Figure 3.**   Modeled and observed daily total transpiration. Observations are derived from field observations
749 of sap flux velocity (see Section 3). (a,b) Modeled (lines, monthly mean) and observed (dots, daily total)
750 transpiration over time. (c-f) Modeled versus observed daily transpiration (mm/d).

Figure 4. Modeled and observed daily total transpiration. Observations are derived from field observations of sap flux velocity (see Section 3). (a,b) Modeled (lines, monthly mean) and observed (dots, daily total) transpiration over time. (c-f) Modeled versus observed daily transpiration (mm/d).
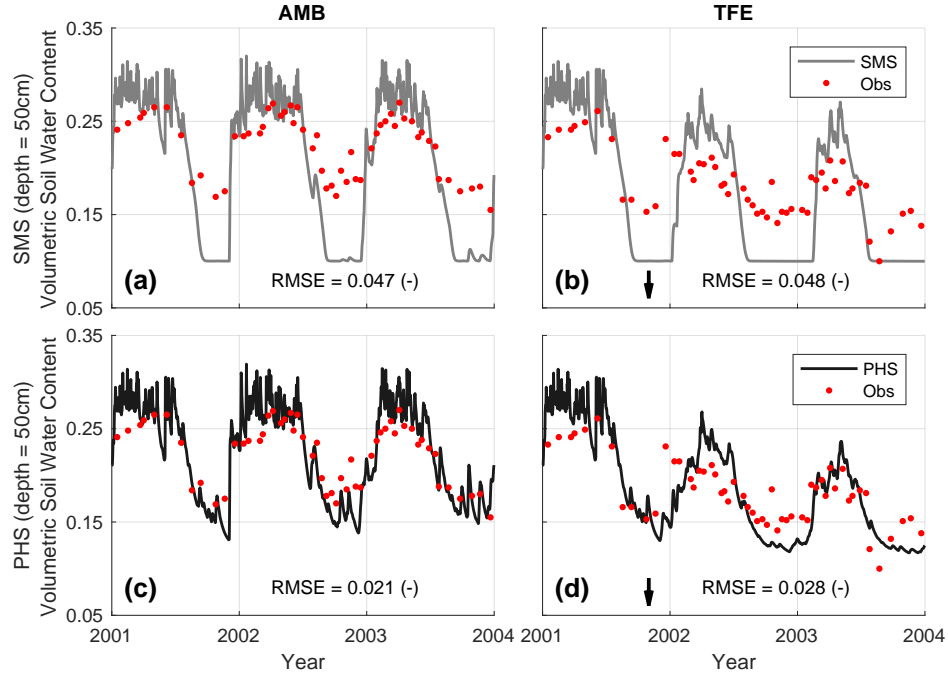
Figure 5. Volumetric soil water content (-) over time under ambient and TFE conditions at depth of 50cm. (a/b) SMS (c/d) PHS. RMSE are 0.048, 0.049, 0.022, and 0.029 [move to plot]. Arrows indicate start of TFE. Figure A.10 shows the same plots at 7 other soil depths.
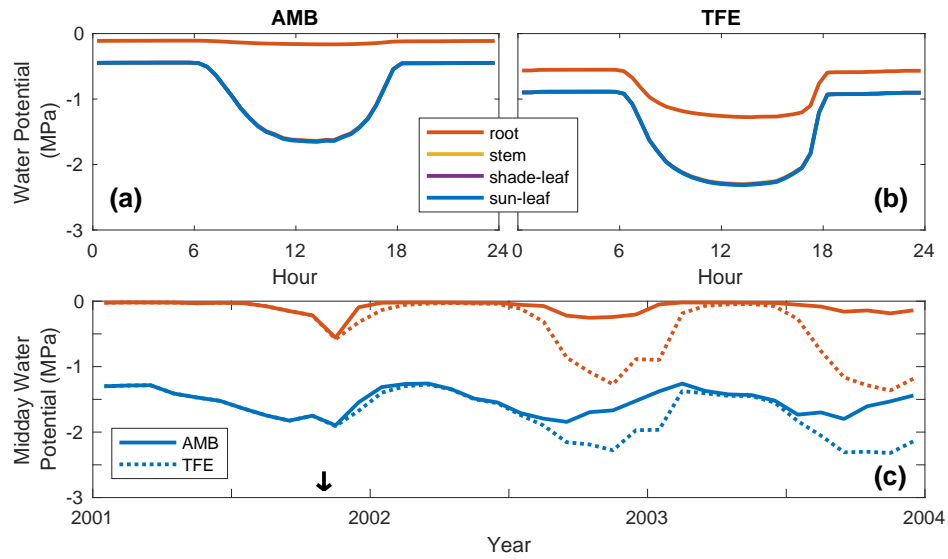
Figure 6. (a,b) 2003 dry season diurnal mean of modeled vegetation water potential under ambient and 60% TFE conditions. Curves are drawn for sunlit leaf, shaded leaf, stem, and root water potentials, with the latter three overlapping. (c) Monthly mean midday (12h-14h) vegetation water potential under ambient (solid line) and TFE (dotted line) conditions. Here curves are drawn only for sunlit leaf and root water potential. Note that TFE begins Nov 1, 2001, as indicated by the vertical arrow.
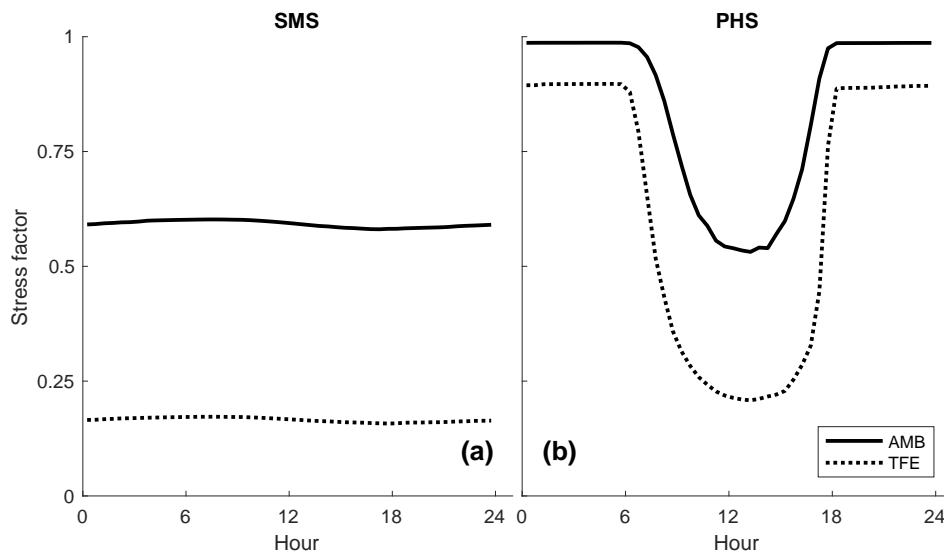
Figure 7. 2003 dry season (SON) diurnal mean water stress function for (a) SMS, and (b) PHS. Note that the water stress factor equals 1 when there is no stress and 0 when fully stressed.
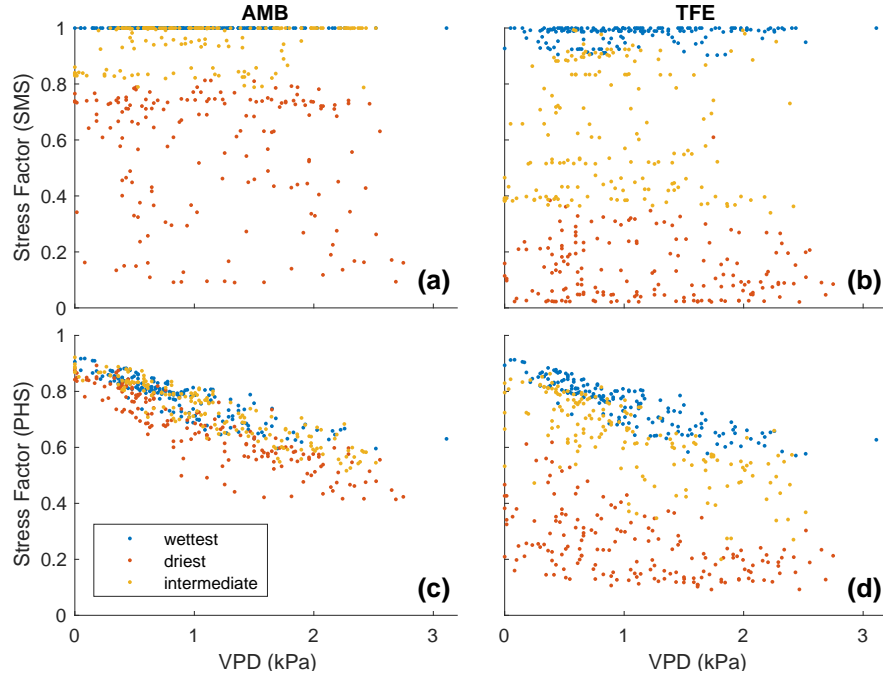
Figure 8. Water stress factor versus vapor pressure deficit (2002-2003), constrained to timesteps with downwelling shortwave radiation between 400 and 425 W/m2 (n=515). Radiation is controlled to highlight the relationship with VPD, the reverse (controlling for VPD) is shown in Figure A.4. For SMS (a,b), data are subdivided based on average soil matric potential, weighted by root fraction. For PHS (c,d), data are subdivided based on predawn (5h) root water potential. Blue dots represent the wettest tercile, yellow dots represent the intermediate tercile, and red dots represent the driest tercile (values defining each tercile are in Table 2).
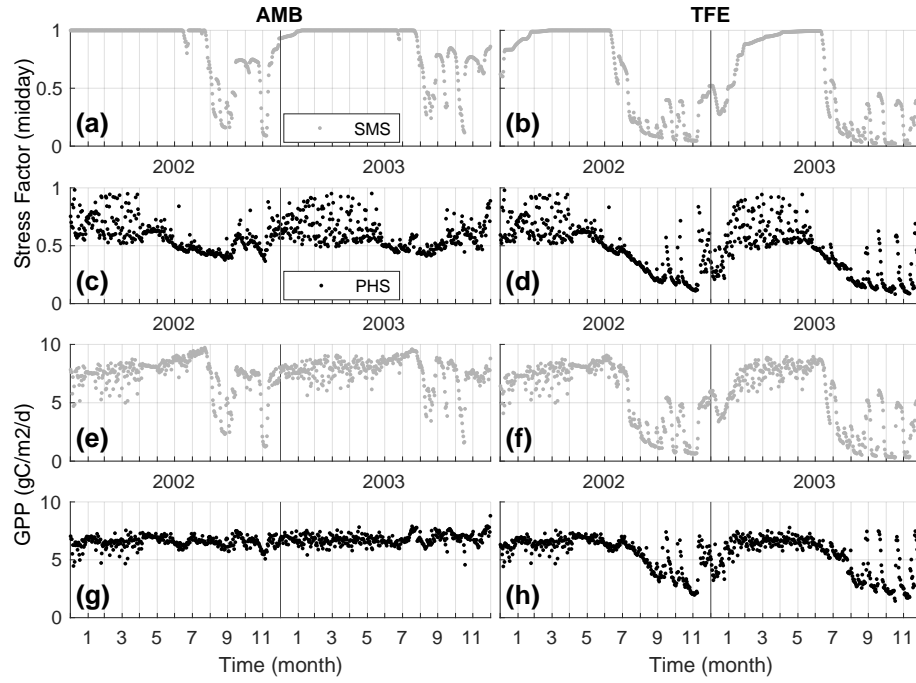
Figure 9. Daily stress factor (midday, averaged over 12h-14h) and GPP during 2002-2003 under ambient (left column) and TFE (right column) conditions. Output from the SMS configuration (a,b,e,f) are plotted with gray color, while output from the PHS configuration (c,d,g,h) are plotted in black.
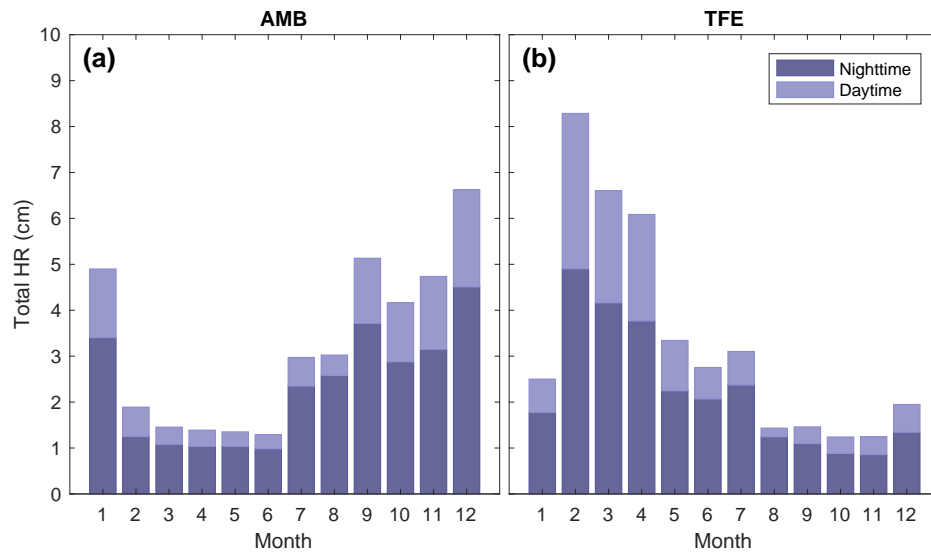
Figure 10. Total hydraulic redistribution (cm) by month across 2003. For (a) ambient through-fall condi-
tions, and (b) 60% throughfall exclusion. Darker shading shows portion of HR at night [6pm,6am], lighter
shading shows portion of HR during day [6am,6pm]. Total HR refers to the sum of all negative root water
uptake flows, when water is deposited by roots into a given soil layer.
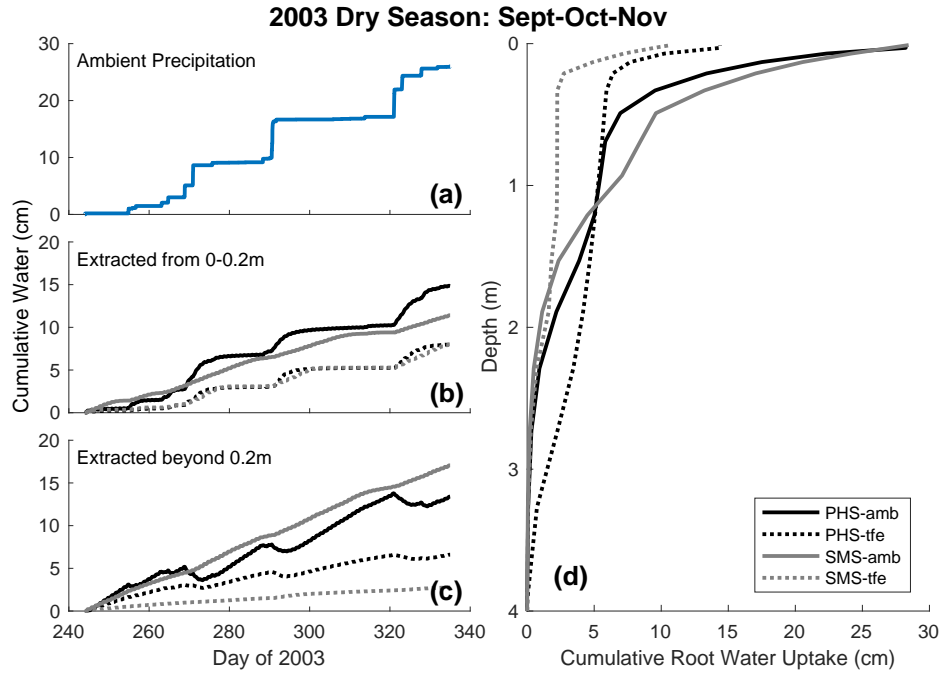
Figure 11. 2003 dry season (SON) cumulative root water uptake and precipitation. (a) Cumulative precipitation over time under ambient conditions (b,c) Cumulative water uptake over time from above and below 0.2m, respectively. (d) Cumulative root water uptake with depth.
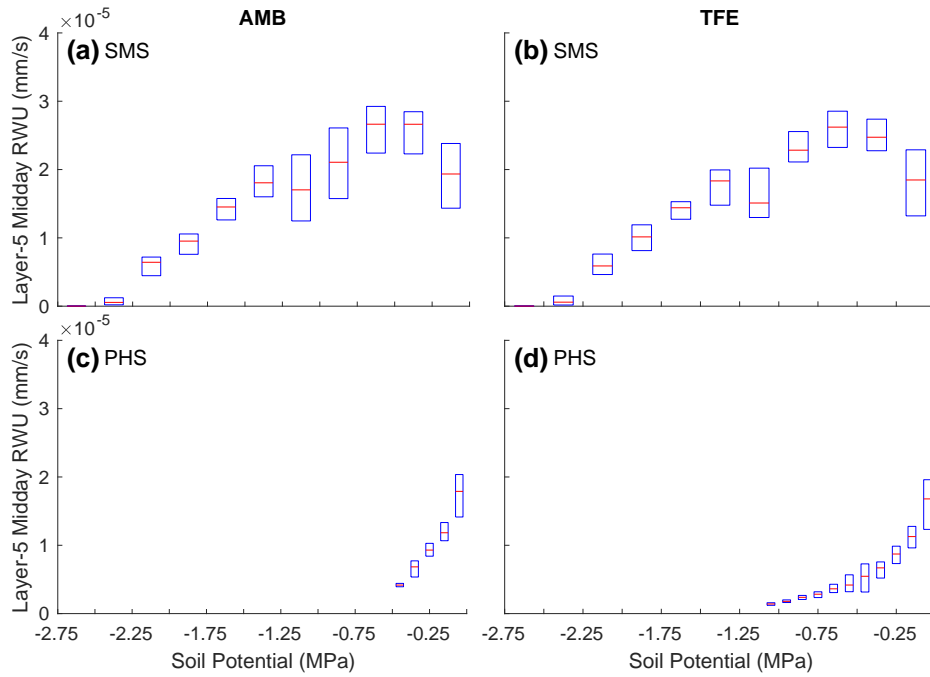
Figure 12. Binned boxplot of root water uptake versus soil potential for Soil Layer 5 (2002-3). Red lines mark the median, with boxes spanning the interquartile range. Bin widths are 0.25 MPa for SMS and 0.1 MPa for PHS. Soil Layer 5 is shown, because it is close enough to the surface (20 to 32 cm) to experience a significant range in soil potential, and it has a large root fraction (14.4%, only Soil Layer 6 has a larger root fraction). Only midday (12h-14h) timesteps are used to highlight the relationship with soil potential.
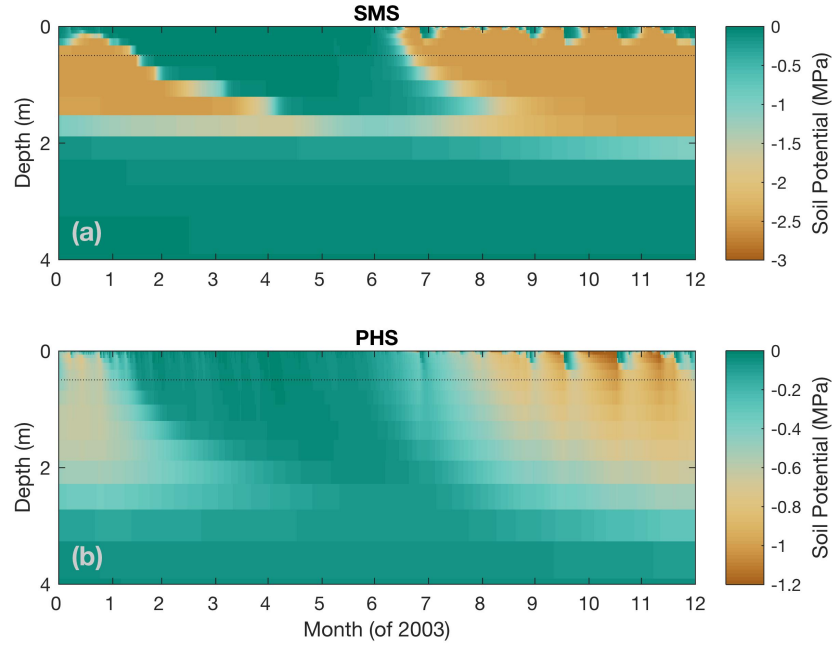
Figure 13. Vertical profile of soil water potential (MPa) over time under 60% throughfall exclusion, for
(a) SMS, and (b) PHS. Note that color axes are different. SMS soil potential spends long periods at -2.5MPa,
which is the value of soil-wilting parameter, ψ_c. Figure 5 subsets this data at 0.5m depth (dotted line), plotted
alongside observations. Soil potential under ambient conditions is shown in Supp Fig A.9.
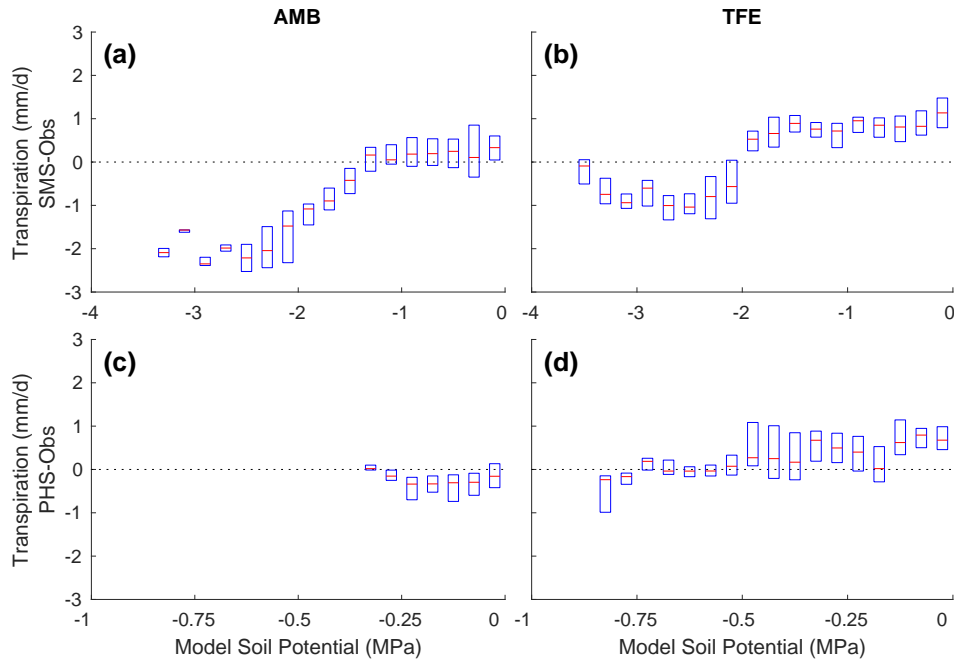
Figure 14. Binned boxplot showing the difference between modeled and observed transpiration (mm/d) versus model soil potential. Red lines are drawn at the median, with boxes spanning the interquartile range. The two models use different root water uptake paradigms, from which we define different operators for column effective soil potential. For SMS we average over the soil column weighted by root fraction and over time (daily mean). For PHS we use predawn (5h) root water potential. Bin widths are 0.2 MPa for SMS (a,b) and 0.05 MPa for PHS (c,d); note the different x-axes.

A: Supplementary Figures
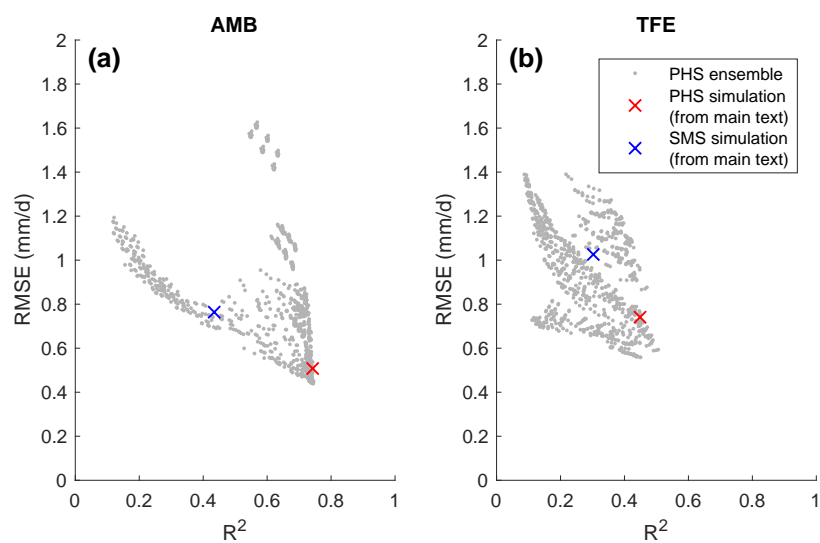
Figure A.1. Parameter tuning exercise.
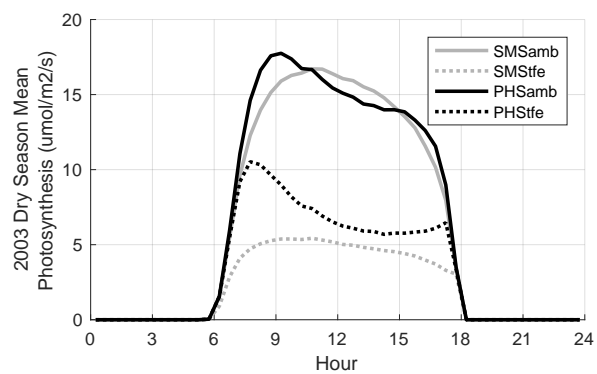
798   **Figure A.2.**   2003 dry season diurnal mean photosynthesis under ambient and TFE conditions for the two
799   model configurations.
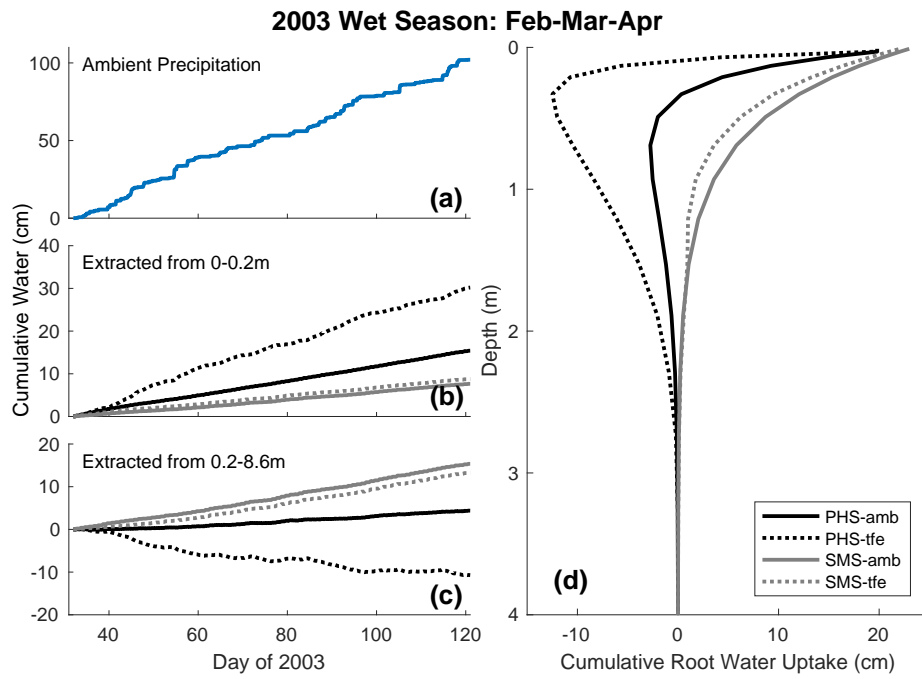
Figure A.3. 2003 wet season (FMA) cumulative root water uptake and precipitation. (a) Cumulative precipitation over time under ambient conditions (b,c) Cumulative water uptake over time from above and below 0.2m, respectively. (d) Cumulative root water uptake with depth.
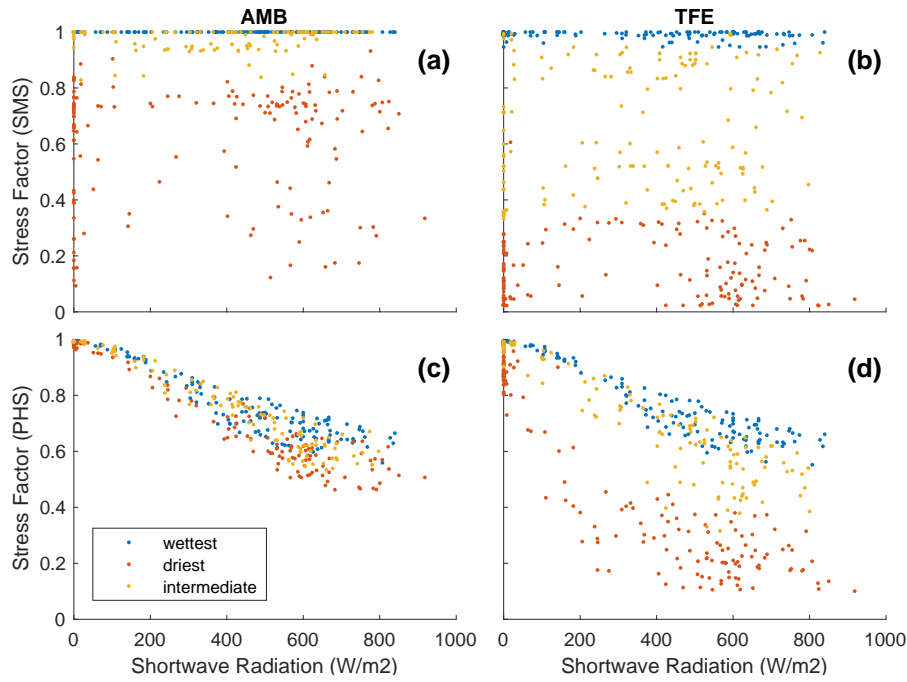
Figure A.4. Water stress factor versus downwelling shortwave radiation (2002-2003), for timesteps with VPD between 1 and 1.0559 kPa (n=470). VPD is controlled to highlight the relationship with downwelling radiation, the reverse (controlling for radiation) is shown in Figure 8. For SMS (a,b), data are subdivided based on average soil matric potential, weighted by root fraction. For PHS (c,d), data are subdivided based on predawn (5h) root water potential. Blue dots represent the wettest tercile, yellow dots represent the intermediate tercile, and red dots represent the driest tercile.
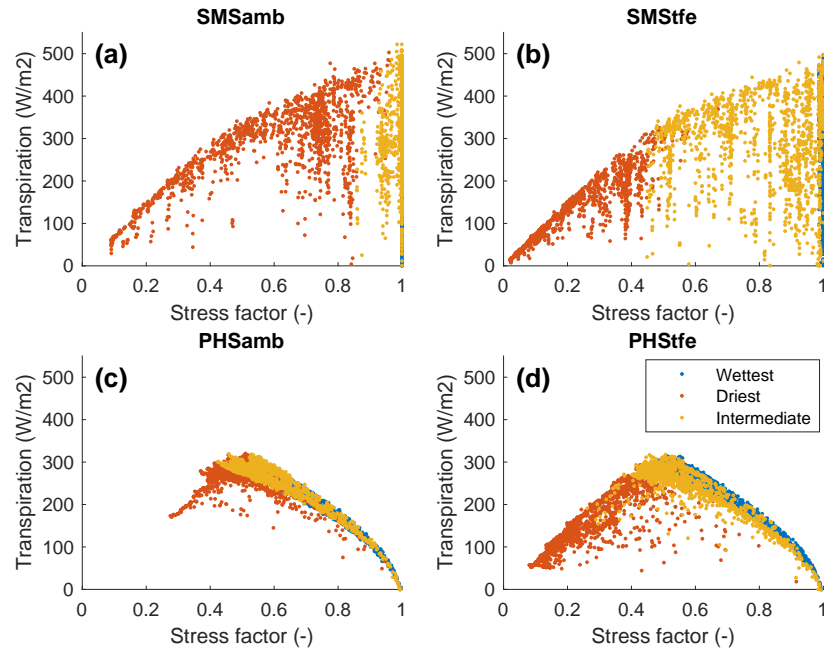
Figure A.5. Midday transpiration vs. stress. Data are colored by soil potential, subdivided into wettest, driest, and intermediate terciles.
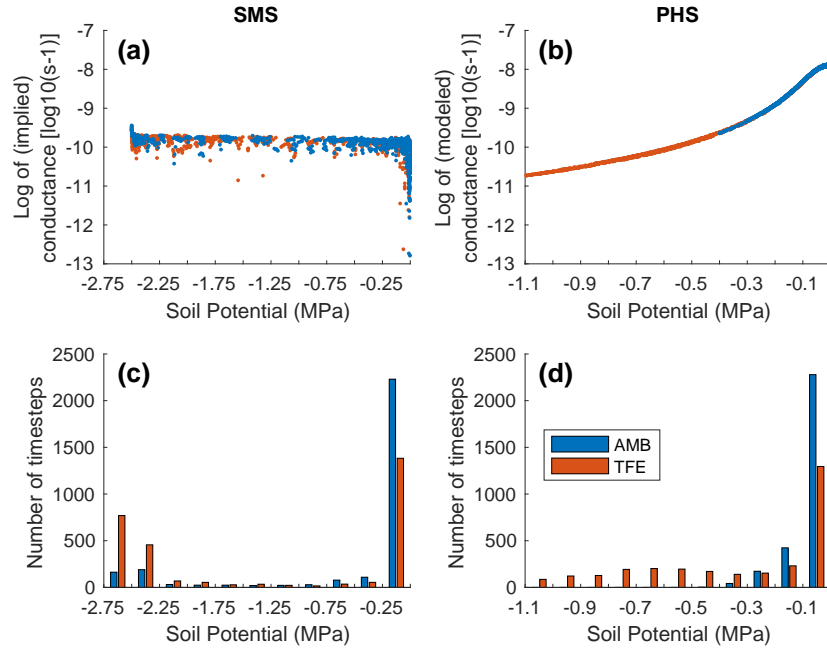
Figure A.6. Log of conductance versus soil potential for Soil Layer 5 (2002-3). Only midday (12h-14h) timesteps are shown to emphasize the relationship with soil potential. With SMS, conductance is not modeled explicitly, but rather calculated as $k=q/\Delta\psi$ (see Section zqz). Beyond 2.5MPa, SMS implied conductance equals 0. PHS conductance captures both root tissue and soil matrix resistances (operating in series).
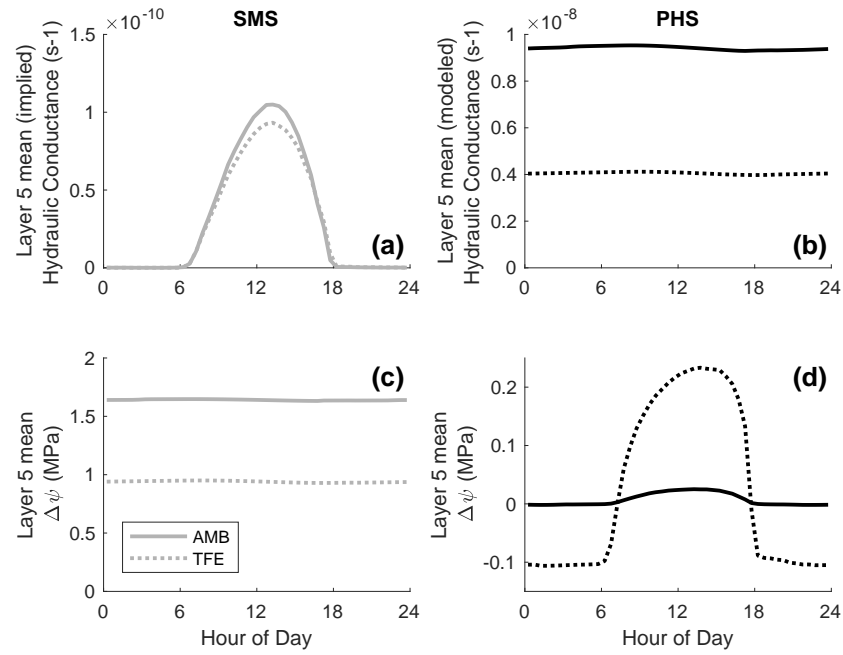
Figure A.7. 2003 diurnal mean of Soil Layer 5 conductance and $\Delta\psi$, under ambient and TFE conditions.
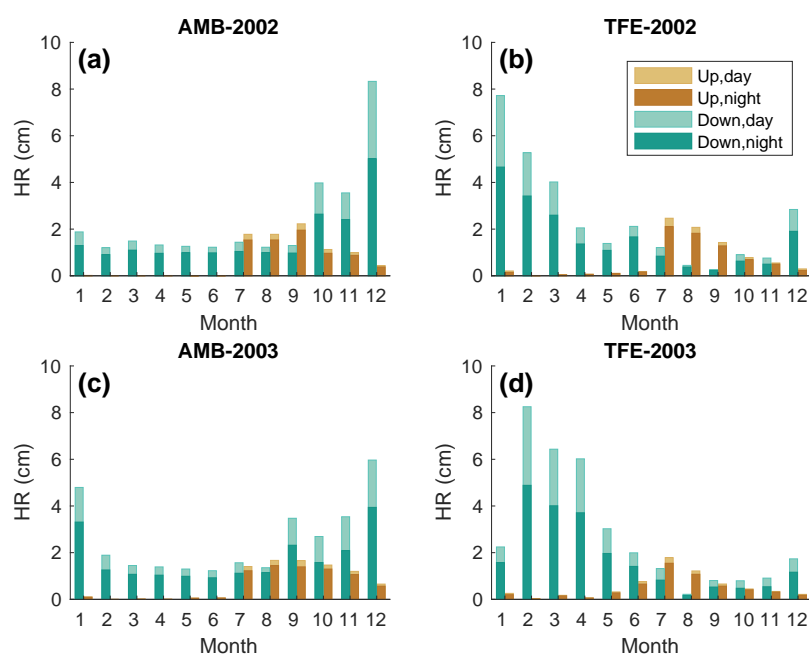
Figure A.8. PHS hydraulic distribution during 2003. Alternative version partitioning by direction.
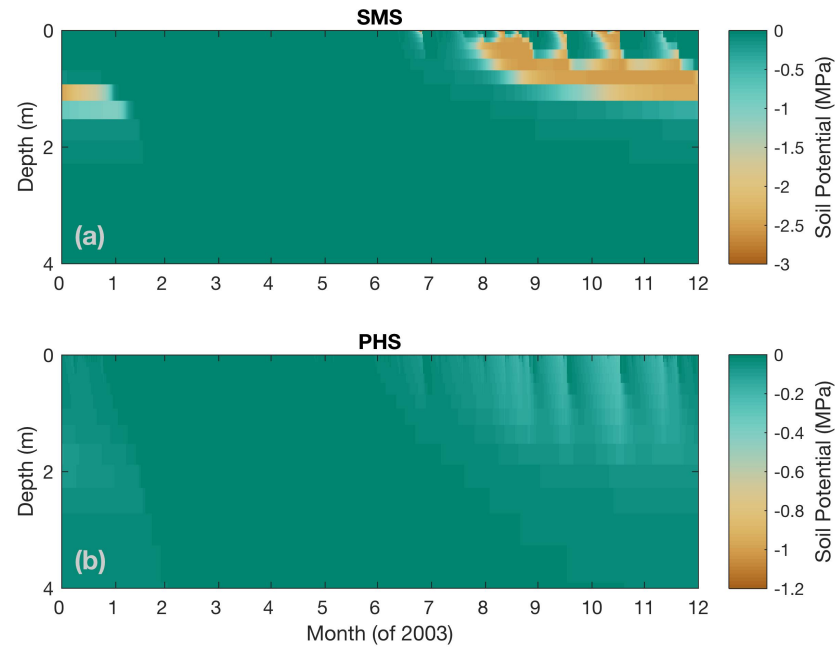
Figure A.9. Vertical profile of soil water potential (MPa) through time under ambient through-fall condi-
tions, for (a) PHS, and (b) SMS. Note that color axes are different.
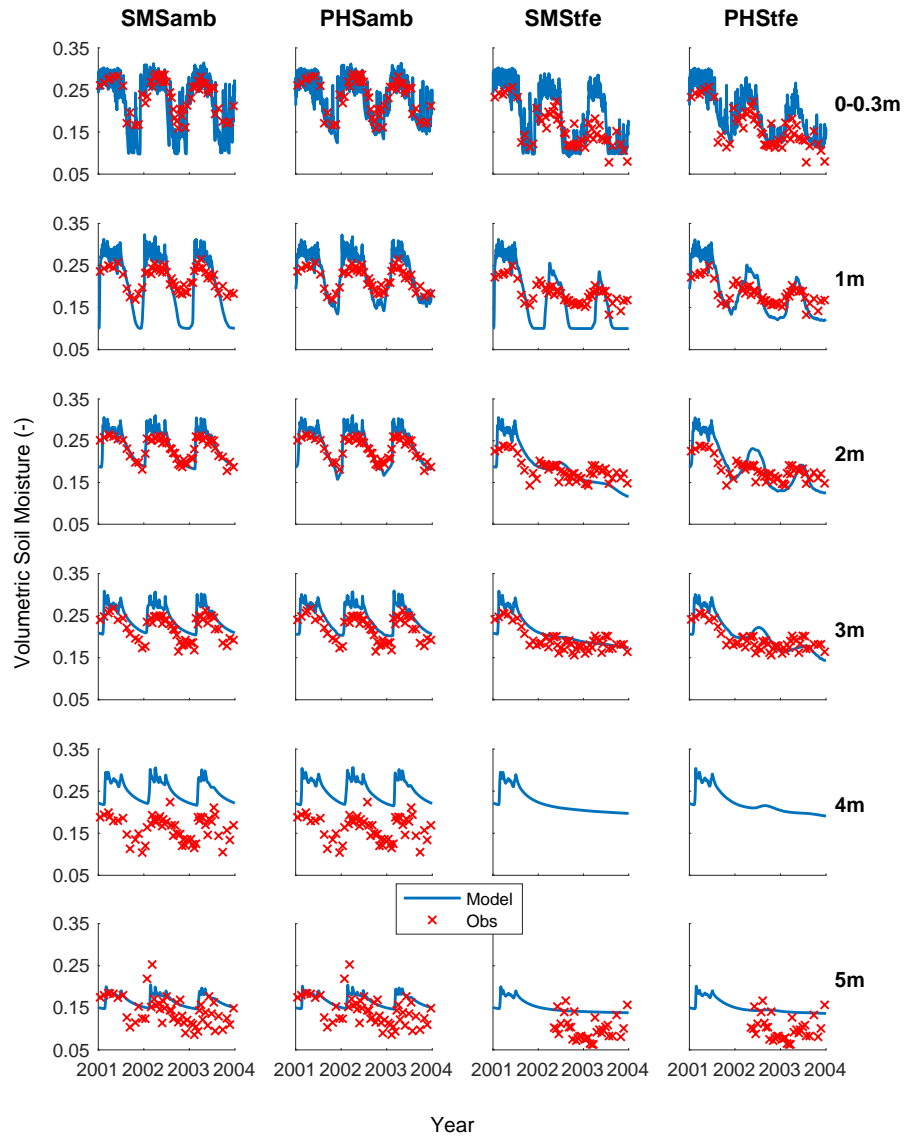
Figure A.10. Time series of soil moisture by soil layer. Complements Figure 13
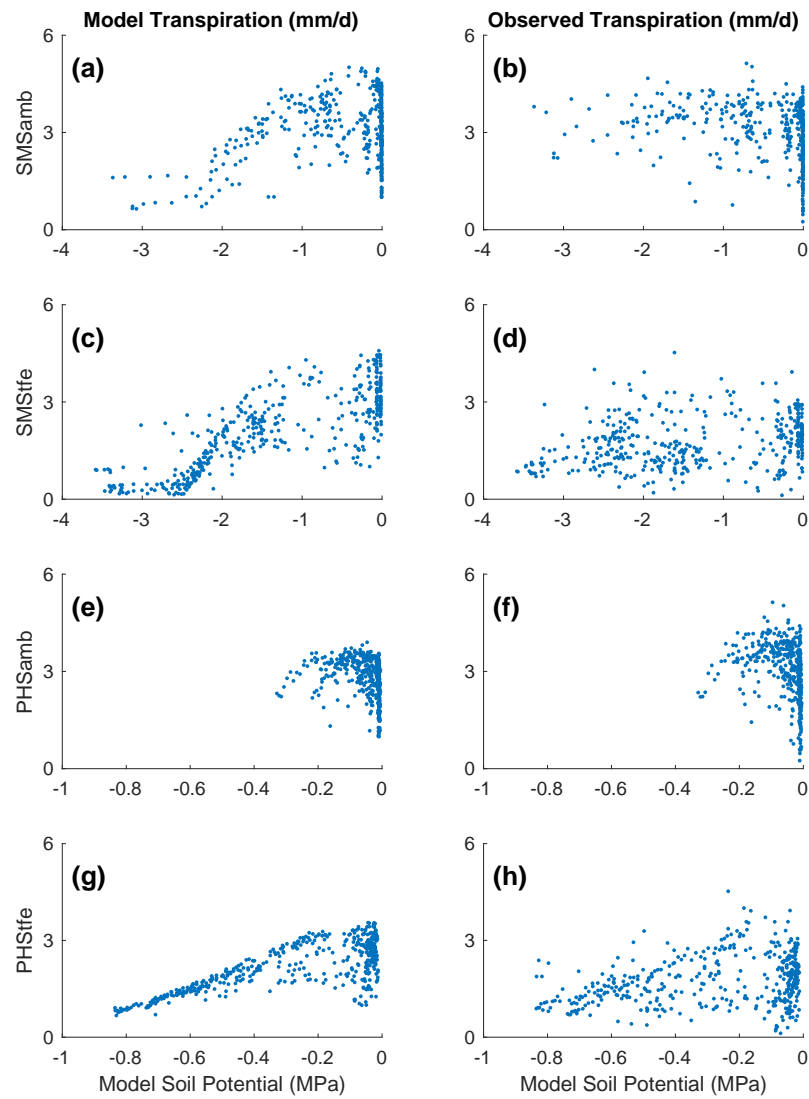
Figure A.11. Modeled (left column) and observed (right column) transpiration vs. model soil potential. Complements Figure 14

B: Appendix to Model Description

B.1 Details of Water Supply

PHS resolves flow across four different segments, soil-to-root, root-to-stem, stem-to-leaf, and leaf-to-transpiration.

Stem-to-leaf. The area bases are sunlit and shaded leaf area, respectively. Note that gravity is assumed negligible here. Likewise there is no length scaling applied to maximum conductance. Therefore the input parameters for $k_{1,\max}$ should be conductances (s^{-1}).

$$q_{1a} = k_1 \cdot \text{LAI-sun} \cdot (\psi_{\text{stem}} - \psi_{\text{sun-leaf}})$$
$$q_{1b} = k_1 \cdot \text{LAI-shade} \cdot (\psi_{\text{stem}} - \psi_{\text{shade-leaf}})$$

(B.1)

$$k_1 = k_{1,\max} \cdot f(\psi_{\text{stem}})$$

(B.2)

$$f(\psi) = 2^{-\left(\frac{\psi}{p_{50}}\right)^{c_k}}$$

(B.3)

Root-to-stem. The area basis is stem area index. The parameter is maximum stem xylem conductivity ($K_{2,\max}$). Stem conductance (k_2) is the result of scaling maximum conductivity by the tree height (h) and applying loss relative to maximum conductance via the vulnerability curve $f(\psi_{\text{root}})$.

$$q_2 = k_2 \cdot \text{SAI} \cdot (\psi_{\text{root}} - \psi_{\text{stem}} - \rho g h)$$

(B.4)

$$k_2 = \frac{K_{2,\max}}{h} \cdot f(\psi_{\text{root}})$$

(B.5)

Soil-to-root. Area basis is RAI in soil layer i, which is based on the layer root fraction times the total root area. Total root area we have as the summed stem and leaf area indices multiplied by a relative root area parameter (f_{root}). The vertical root distribution is defined by the layer root fraction (r_i), which follows a one-parameter (by PFT) power law decay following *Jackson et al.* [1996].

$$q_{3,i} = k_{3,i} \cdot \text{RAI}_i \cdot (\psi_{\text{soil,i}} - \psi_{\text{root}} - \rho g z_i)$$

(B.6)

$$\text{RAI}_i = f_{\text{root}} \cdot (\text{SAI} + \text{LAI}) \cdot r_i$$

(B.7)

$$k_{3,i} = \frac{k_{r,i} + k_{s,i}}{k_{r,i} \cdot k_{s,i}}$$

(B.8)

$$k_{r,i} = \frac{K_{r,\max}}{l_i} f(\psi_{\text{soil,i}})$$

(B.9)

$$l_i = z_i + x$$

(B.10)

$$k_{s,i} = \frac{K_{s,i}}{d}$$

(B.11)

The conductance $k_{3,i}$ reflects two resistors in series, from soil-to-root ($k_{s,i}$) and through the root tissue ($k_{r,i}$). The root tissue conductance is attenuated via the vulnerability curve framework. The input parameter is maximum root xylem conductivity, on the basis of RAI as defined above. The root conductivity is scaled by the conducting length, which is estimated as the sum of soil layer depth (z_i) and average lateral extent (x, static parameter). The soil conductivity $K_{s,i}$ is calculated from the layer soil matric potential (ψ_s) and soil properties following *Clapp and Hornberger* [1978] as described in *Oleson et al.* [2013]. The soil conductance ($k_{s,i}$) is the result of scaling the conductivity by d, the distance between roots estimated following *Williams et al.* [1996] and *Bonan et al.* [2014]

The challenge here is obviously getting your head around all the parameters.

B.2 Details of Water Demand

The CLM5 implementation utilizes the Medlyn stomatal conductance model [*Medlyn et al.*, 2011], while also applying water stress through V_{cmax}. Transpiration is calculated reflecting contributions from both stomatal conductance and leaf boundary layer conductance (g_b).

$$V_{cmax} = f_w \, V_{cmax,ww} \tag{B.12}$$

$$g_s = g_0 + \left(1 + \frac{g_1}{\sqrt{D}}\right)\frac{A}{C_a} \tag{B.13}$$

$$E_{sun} = g_{s,sun} * \rho * \text{VPD} * lai_{sun} * \left(1 + \frac{g_{s,sun}}{g_b}\right)^{-1}$$
$$E_{shade} = g_{s,shade} * \rho * \text{VPD} * lai_{shade} * \left(1 + \frac{g_{s,shade}}{g_b}\right)^{-1} \tag{B.14}$$

At the beginning of a set of PHS iterations, we solve for $E_{sun,max}$ and $E_{shade,max}$, by running the stomatal conductance scheme with f_w set to 1 (no stress). Within each PHS iteration, we do not resolve the full stomatal conductance scheme, but instead consider only the linear attenuation of stomatal conductance by f_w. Transpiration is attenuated relative to the maximal values according to leaf water potential.

$$E_{sun} = E_{sun,max} * 2^{-\left(\frac{\psi_{leaf}}{\psi_{50}}\right)^{c_k}}$$
$$E_{shade} = E_{shade,max} * 2^{-\left(\frac{\psi_{leaf}}{\psi_{50}}\right)^{c_k}} \tag{B.15}$$

We define f_w as the ratio of attenuated stomatal conductance ($g_{s,sun}$, $g_{s,shade}$) to maximal stomatal conductance ($g_{s,sun,max}$, $g_{s,shade,max}$), where $g_{s,sun,max}$ and $g_{s,shade,max}$ are the stomatal conductance values associated with $E_{sun,max}$ and $E_{shade,max}$. As such, the definition in the main text (Equation 17), represents a linear simplification between f_w, stomatal conductance, and transpiration.

$$f_{w,sun} = \frac{g_{s,sun}}{g_{s,sun,max}}$$
$$f_{w,shade} = \frac{g_{s,shade}}{g_{s,shade,max}} \tag{B.16}$$

After each PHS iteration, we compute $g_{s,sun}$ and $g_{s,shade}$ via Equations B.12 and B.12 (which involves iterating for intercellular CO_2 concentration). We then update $g_{s,sun,max}$ and $g_{s,shade,max}$ to achieve consistency between equations (B.14) and (B.15). At this point $g_{s,sun,max}$ and $g_{s,shade,max}$ no longer refer to the values associated with $f_w = 1$, but rather also incorporate the non-linearity between g_s and f_w. The PHS iteration continues to convergence of f_w (see Figure B.1). The numerics have proven to be stable in practice, but future versions may aim to better integrate PHS within the stomatal conductance scheme to improve the coherence of Equations 17 and B.16.

$$g_{s,sun,max} = \frac{g_{s,sun}}{f_{w,sun}}$$
$$g_{s,shade,max} = \frac{g_{s,shade}}{f_{w,shade}} \tag{B.17}$$

Calculate metabolic parameters
$(V_{cmax}, J_{max}, R_d, K_c, K_o, \Gamma_*)$ ← Initial T_l

Initial C_i

Set $f_{w,sun}$ and $f_{w,shade}$ = 1

Calculate assimilation $(A_{n,max})$, stomatal conductance $(g_{s,sun,max}, g_{s,shade,max})$,
transpiration $(T_{sun,max}, T_{shade,max})$ [absent water stress]

Calculate C_i

c_i convergence? — no

Initial C_i

PHS solves for ψ and f_w

Calculate assimilation (A_n) and stomatal conductance $(g_{s,sun}, g_{s,shade})$
using f_w [includes water stress]

Calculate C_i

c_i convergence? — no

f_w convergence? — no

Update
$g_{s,sun,max}$ & $g_{s,shade,max}$

Calculate leaf temperature (T_l) and fluxes $(H_l, \lambda E_l)$

no — T_l convergence?

Figure B.1. Flow chart of PHS iterative solution

888

B.3 Details of Water Potential Solution

The continuity of water flow through the system yields four equations

$$E_{sun} = q_{1a}$$
$$E_{shade} = q_{1b}$$
$$q_{1a} + q_{1b} = q_2 \tag{B.18}$$
$$q_2 = \sum_{i=1}^{nlevsoi} q_{3,i}$$

We seek the set of vegetation water potential values (four unknowns),

$$\psi = \begin{bmatrix} \psi_{sunleaf} \\ \psi_{shadeleaf} \\ \psi_{stem} \\ \psi_{root} \end{bmatrix} \tag{B.19}$$

that satisfies these equations, as forced by the soil moisture and atmospheric state.

Each flux on the schematic can be represented in terms of the relevant water potentials.

Defining the transpiration fluxes:

$$E_{sun} = E_{sun,max} \cdot 2^{-\left(\frac{\psi_{sunleaf}}{p50_e}\right)^{c_k}}$$
$$\tag{B.20}$$
$$E_{shade} = E_{shade,max} \cdot 2^{-\left(\frac{\psi_{shadeleaf}}{p50_e}\right)^{c_k}}$$

Defining the water supply fluxes:

$$q_{1a} = k_{1a,max} \cdot 2^{-\left(\frac{\psi_{stem}}{p50_1}\right)^{c_k}} \cdot \text{LAI}_{sun} \cdot \left(\psi_{stem} - \psi_{sunleaf}\right)$$
$$q_{1b} = k_{1b,max} \cdot 2^{-\left(\frac{\psi_{stem}}{p50_1}\right)^{c_k}} \cdot \text{LAI}_{shade} \cdot \left(\psi_{stem} - \psi_{shadeleaf}\right)$$
$$\tag{B.21}$$
$$q_2 = \frac{k_{2,max}}{z_2} \cdot 2^{-\left(\frac{\psi_{root}}{p50_2}\right)^{c_k}} \cdot SAI \cdot (\psi_{root} - \psi_{stem} - \Delta\psi_z)$$
$$q_{soil} = \sum_{i=1}^{nlevsoi} q_{3,i} = \sum_{i=1}^{nlevsoi} k_{3,i} \cdot RAI \cdot (\psi_{soil,i} - \psi_{root} + \Delta\psi_{z,i})$$

We're looking to find the vector ψ that fits with soil and atmospheric forcings while satisfying water flow continuity. Due to the model non-linearity, we use a linearized explicit approach, iterating with Newton's method. The initial guess is the solution for ψ (vector) from the previous time step. The general framework, from iteration m to $m + 1$ is:

$$q^{m+1} = q^m + \frac{\delta q}{\delta \psi} \Delta\psi$$
$$\tag{B.22}$$
$$\psi^{m+1} = \psi^m + \Delta\psi$$

So for our first flux balance equation, at iteration $m + 1$, we have:

$$E_{sun}^{m+1} = q_{1a}^{m+1} \tag{B.23}$$

Which can be linearized to:

$$E_{sun}^{m} + \frac{\delta E_{sun}}{\delta \psi}\Delta\psi = q_{1a}^{m} + \frac{\delta q_{1a}}{\delta \psi}\Delta\psi \tag{B.24}$$

And rearranged to be:

$$\frac{\delta q_{1a}}{\delta \psi}\Delta\psi - \frac{\delta E_{sun}}{\delta \psi}\Delta\psi = E_{sun}^{m} - q_{1a}^{m} \tag{B.25}$$

And for the other 3 flux balance equations:

$$\frac{\delta q_{1b}}{\delta \psi}\Delta\psi - \frac{\delta E_{sha}}{\delta \psi}\Delta\psi = E_{sha}^{m} - q_{1b}^{m}$$
$$\frac{\delta q_2}{\delta \psi}\Delta\psi - \frac{\delta q_{1a}}{\delta \psi}\Delta\psi - \frac{\delta q_{1b}}{\delta \psi}\Delta\psi = q_{1a}^{m} + q_{1b}^{m} - q_2^{m} \tag{B.26}$$
$$\frac{\delta q_{soil}}{\delta \psi}\Delta\psi - \frac{\delta q_2}{\delta \psi}\Delta\psi = q_2^{m} - q_{soil}^{m}$$

Putting all four together in matrix form:

$$\begin{bmatrix} \dfrac{\delta q_{1a}}{\delta \psi} - \dfrac{\delta E_{sun}}{\delta \psi} \\ \dfrac{\delta q_{1b}}{\delta \psi} - \dfrac{\delta E_{sha}}{\delta \psi} \\ \dfrac{\delta q_2}{\delta \psi} - \dfrac{\delta q_{1a}}{\delta \psi} - \dfrac{\delta q_{1b}}{\delta \psi} \\ \dfrac{\delta q_{soil}}{\delta \psi} - \dfrac{\delta q_2}{\delta \psi} \end{bmatrix} \Delta\psi = \begin{bmatrix} E_{sun}^{m} - q_{1a}^{m} \\ E_{sha}^{m} - q_{1b}^{m} \\ q_{1a}^{m} + q_{1b}^{m} - q_2^{m} \\ q_2^{m} - q_{soil}^{m} \end{bmatrix} \tag{B.27}$$

Now to expand the left-hand side, from vector ψ to the four distinct plant water potential nodes, noting that many derivatives are zero (e.g. $\dfrac{\delta E_{sun}}{\delta \psi_{sha}} = 0$)

Introducing the notation: $A\Delta\psi = b$

$$\Delta\psi = \begin{bmatrix} \Delta\psi_{sunleaf} \\ \Delta\psi_{shadeleaf} \\ \Delta\psi_{stem} \\ \Delta\psi_{root} \end{bmatrix} \tag{B.28}$$

$$A = \begin{bmatrix} \dfrac{\delta q_{1a}}{\delta \psi_{sun}} - \dfrac{\delta E_{sun}}{\delta \psi_{sun}} & 0 & \dfrac{\delta q_{1a}}{\delta \psi_{stem}} & 0 \\ 0 & \dfrac{\delta q_{1b}}{\delta \psi_{sha}} - \dfrac{\delta E_{sha}}{\delta \psi_{sha}} & \dfrac{\delta q_{1b}}{\delta \psi_{stem}} & 0 \\ -\dfrac{\delta q_{1a}}{\delta \psi_{sun}} & -\dfrac{\delta q_{1b}}{\delta \psi_{sha}} & \dfrac{\delta q_2}{\delta \psi_{stem}} - \dfrac{\delta q_{1a}}{\delta \psi_{stem}} - \dfrac{\delta q_{1b}}{\delta \psi_{stem}} & \dfrac{\delta q_2}{\delta \psi_{root}} \\ 0 & 0 & -\dfrac{\delta q_2}{\delta \psi_{stem}} & \dfrac{\delta q_{soil}}{\delta \psi_{root}} - \dfrac{\delta q_2}{\delta \psi_{root}} \end{bmatrix} \tag{B.29}$$

$$b = \begin{bmatrix} E^m_{sun} - q^m_{b1} \\ E^m_{sha} - q^m_{b2} \\ q^m_{b1} + q^m_{b2} - q^m_{stem} \\ q^m_{stem} - q^m_{soil} \end{bmatrix} \tag{B.30}$$

Now we compute all the entries for *A* and *b* based on the soil moisture and maximum transpiration forcings and can solve to find:

$$\Delta\psi = A^{-1}b \tag{B.31}$$

$$\psi_{m+1} = \psi_m + \Delta\psi \tag{B.32}$$

We iterate until $b \rightarrow 0$, signifying water flux balance through the system. The result is a final set of water potentials ($\psi_{root}, \psi_{xylem}, \psi_{shadeleaf}, \psi_{sunleaf}$) satisfying non-divergent water flux through the system.

B.4 Parameter tuning exercise

We used a factorial design to create 972 ensemble members based on the parameter values below. We ran PHS simulations under both AMB and TFE conditions. All simulations used the same initial conditions, which were the result of a previous simulation. We evaluated the ensemble members based on the fit to sap flux observations, selecting that which maximized $R^2_{amb} + R^2_{tfe} - RMSE_{amb} - RMSE_{tfe}$ (Supp Fig A.1).

Stem conductivity, k_{max}: 2e-8, 4e-8, 8e-8 s^{-1}
Root conductivity, $k_{r,max}$: 2e-9, 6e-8, 18e-9 s^{-1}
Root and stem vulnerability ψ_{50}: -1.75, -2.25, -2.75 MPa
Stomatal ψ_{50}: above plus either 0 or 0.5MPa
Vulnerability shape parameter, c_k: 2.95, 3.95, 5.45 (unitless)
Medlyn slope, g_1: 6, 7 kPa$^{0.5}$
Rooting depth parameter, β: 0.95, 0.98, 0.993 (unitless)

Acknowledgments

References

Allen, C. D., A. K. Macalady, H. Chenchouni, D. Bachelet, N. McDowell, M. Vennetier, T. Kitzberger, A. Rigling, D. D. Breshears, E. T. Hogg, P. Gonzalez, R. Fensham, Z. Zhang, J. Castro, N. Demidova, J.-H. Lim, G. Allard, S. W. Running, A. Semerci, and N. Cobb (2010), A global overview of drought and heat-induced tree mortality reveals emerging climate change risks for forests, *Forest Ecology and Management*, *259*(4), 660 – 684, doi:https://doi.org/10.1016/j.foreco.2009.09.001.

Anderegg, W. R. L. (2015a), Spatial and temporal variation in plant hydraulic traits and their relevance for climate change impacts on vegetation, *New Phytologist*, *205*(3), 1008–1014, doi:10.1111/nph.12907.

Anderegg, W. R. L., J. M. Kane, and L. D. L. Anderegg (2013a), Consequences of widespread tree mortality triggered by drought and temperature stress, *Nature Climate Change*, *3*(1), 30–36.

Anderegg, W. R. L., L. Plavcová, L. D. L. Anderegg, U. G. Hacke, J. A. Berry, and C. B. Field (2013b), Drought's legacy: multiyear hydraulic deterioration underlies widespread

aspen forest die-off and portends increased future risk, *Global Change Biology*, *19*(4), 1188–1196, doi:10.1111/gcb.12100.

Anderegg, W. R. L., C. Schwalm, F. Biondi, J. J. Camarero, G. Koch, M. Litvak, K. Ogle, J. D. Shaw, E. Shevliakova, A. P. Williams, A. Wolf, E. Ziaco, and S. Pacala (2015b), Pervasive drought legacies in forest ecosystems and their implications for carbon cycle models, *Science*, *349*(6247), 528–532, doi:10.1126/science.aab1833.

Anderegg, W. R. L., A. Wolf, A. Arango-Velez, B. Choat, D. J. Chmura, S. Jansen, T. Kolb, S. Li, F. Meinzer, P. Pita, V. Resco de Dios, J. S. Sperry, B. T. Wolfe, and S. Pacala (2017), Plant water potential improves prediction of empirical stomatal models, *PLOS ONE*, *12*(10), 1–17, doi:10.1371/journal.pone.0185481.

Bartlett, M. K., T. Klein, S. Jansen, B. Choat, and L. Sack (2016), The correlations and sequence of plant stomatal, hydraulic, and wilting responses to drought, *Proceedings of the National Academy of Sciences*, *113*(46), 13,098–13,103, doi:10.1073/pnas.1604088113.

Bohrer, G., H. Mourad, T. A. Laursen, D. Drewry, R. Avissar, D. Poggi, R. Oren, and G. G. Katul (2005), Finite element tree crown hydrodynamics model (fetch) using porous media flow within branching elements: A new representation of tree hydrodynamics, *Water Resources Research*, *41*(11), doi:10.1029/2005WR004181.

Bonan, G. B. (2008), Forests and climate change: Forcings, feedbacks, and the climate benefits of forests, *Science*, *320*(5882), 1444–1449, doi:10.1126/science.1155121.

Bonan, G. B., P. J. Lawrence, K. W. Oleson, S. Levis, M. Jung, M. Reichstein, D. M. Lawrence, and S. C. Swenson (2011), Improving canopy processes in the Community Land Model version 4 (CLM4) using global flux fields empirically inferred from FLUXNET data, *Journal of Geophysical Research*, *116*, doi:10.1029/2010JG001593.

Bonan, G. B., M. Williams, R. A. Fisher, and K. W. Oleson (2014), Modeling stomatal conductance in the earth system: linking leaf water-use efficiency and water transport along the soil-plant-atmosphere continuum, *Geoscientific Model Development*, *7*(5), 2193–2222, doi:10.5194/gmd-7-2193-2014.

Bouda, M., and J. E. Saiers (2017), Dynamic effects of root system architecture improve root water uptake in 1-d process-based soil-root hydrodynamics, *Advances in Water Resources*, *110*, 319 – 334, doi:https://doi.org/10.1016/j.advwatres.2017.10.018.

Boyer, J. S. (1967), Leaf water potentials measured with a pressure chamber, *Plant Physiology*, *42*(1), 133–137, doi:10.1104/pp.42.1.133.

Brooks, J. R., F. C. Meinzer, J. M. Warren, J.-C. Domec, and R. Coulombe (2006), Hydraulic redistribution in a douglas-fir forest: lessons from system manipulations, *Plant, Cell & Environment*, *29*(1), 138–150, doi:10.1111/j.1365-3040.2005.01409.x.

Burgess, S. S. O., M. A. Adams, N. C. Turner, and C. K. Ong (1998), The redistribution of soil water by tree root systems, *Oecologia*, *115*(3), 306–311, doi:10.1007/s004420050521.

Cai, G., J. Vanderborght, M. Langensiepen, A. Schnepf, H. Hüging, and H. Vereecken (2018), Root growth, water uptake, and sap flow of winter wheat in response to different soil water conditions, *Hydrology and Earth System Sciences*, *22*(4), 2449–2470, doi: 10.5194/hess-22-2449-2018.

Cai, W., S. Borlace, M. Lengaigne, P. Van Rensch, M. Collins, G. Vecchi, A. Timmermann, A. Santoso, M. J. Mcphaden, L. Wu, M. H. England, G. Wang, E. Guilyardi, and F.-f. Jin (2014), Increasing frequency of extreme El Niño events due to greenhouse warming, *Nature Climate Change*, *4*(2), 111–116.

Celia, M. A., E. T. Bouloutas, and R. L. Zarba (1990), A general mass-conservative numerical solution for the unsaturated flow equation, *Water Resources Research*, *26*(7), 1483–1496, doi:10.1029/WR026i007p01483.

Choat, B., S. Jansen, T. J. Brodribb, H. Cochard, S. Delzon, R. Bhaskar, S. J. Bucci, T. S. Feild, S. M. Gleason, U. G. Hacke, A. L. Jacobsen, F. Lens, H. Maherali, J. MartÃŋnez-Vilalta, S. Mayr, M. Mencuccini, P. J. Mitchell, A. Nardini, J. Pittermann, R. B. Pratt, J. S. Sperry, M. Westoby, I. J. Wright, and A. E. Zanne (2012), Global convergence in the vulnerability of forests to drought, *Nature*, *491*(7426), 752–5.

Christoffersen, B. O., M. Gloor, S. Fauset, N. M. Fyllas, D. R. Galbraith, T. R. Baker, B. Kruijt, L. Rowland, R. A. Fisher, O. J. Binks, S. Sevanto, C. Xu, S. Jansen, B. Choat, M. Mencuccini, N. G. McDowell, and P. Meir (2016), Linking hydraulic traits to tropical forest function in a size-structured and trait-driven model (tfs v.1-hydro), *Geoscientific Model Development*, *9*(11), 4227–4255, doi:10.5194/gmd-9-4227-2016.

Clapp, R. B., and G. M. Hornberger (1978), Empirical equations for some soil hydraulic properties, *Water Resources Research*, *14*(4), 601–604, doi:10.1029/WR014i004p00601.

Collatz, G., J. Ball, C. Grivet, and J. A. Berry (1991), Physiological and environmental regulation of stomatal conductance, photosynthesis and transpiration: a model that includes a laminar boundary layer, *Agricultural and Forest Meteorology*, *54*(2), 107 – 136, doi: http://dx.doi.org/10.1016/0168-1923(91)90002-8.

Couvreur, V., J. Vanderborght, and M. Javaux (2012), A simple three-dimensional macroscopic root water uptake model based on the hydraulic architecture approach, *Hydrology and Earth System Sciences*, *16*(8), 2957–2971, doi:10.5194/hess-16-2957-2012.

da Costa, A. C., D. B. Metcalfe, C. E. Doughty, A. A. de Oliveira, G. F. Neto, M. C. da Costa, J. de Athaydes Silva Junior, L. E. Aragão, S. Almeida, D. R. Galbraith, L. M. Rowland, P. Meir, and Y. Malhi (2014), Ecosystem respiration and net primary productivity after 8-10 years of experimental through-fall reduction in an eastern Amazon forest, *Plant Ecology & Diversity*, *7*(1-2), 7–24, doi:10.1080/17550874.2013.798366.

da Costa, A. C. L., D. Galbraith, S. Almeida, B. Takeshi, T. Portela, M. da Costa, J. ao de Athaydes Silva Junior, A. P. Braga, P. H. L. de Gonçalves, A. A. de Oliveira, R. Fisher, O. L. Phillips, D. B. Metcalfe, P. Levy, and P. Meir (2010), Effect of 7 yr of experimental drought on vegetation dynamics and biomass storage of an eastern amazonian rainforest, *The New Phytologist*, *187*(3), 579–591.

Dai, A. (2013), Increasing drought under global warming in observations and models, *Nature Climate Change*, *3*(1), 52–58.

Dai, Y., R. E. Dickinson, and Y.-P. Wang (2004), A two-big-leaf model for canopy temperature, photosynthesis, and stomatal conductance, *Journal of Climate*, *17*(12), 2281–2299, doi:10.1175/1520-0442(2004)017<2281:ATMFCT>2.0.CO;2.

De Kauwe, M. G., J. Kala, Y.-S. Lin, A. J. Pitman, B. E. Medlyn, R. A. Duursma, G. Abramowitz, Y.-P. Wang, and D. G. Miralles (2015), A test of an optimal stomatal conductance scheme within the CABLE land surface model, *Geoscientific Model Development*, *8*(2), 431–452, doi:10.5194/gmd-8-431-2015.

De Kauwe, M. G., B. E. Medlyn, J. Knauer, and C. A. Williams (2017), Ideas and perspectives: how coupled is the vegetation to the boundary layer?, *Biogeosciences*, *14*(19), 4435–4453, doi:10.5194/bg-14-4435-2017.

Domec, J.-C., J. S. King, A. Noormets, E. Treasure, M. J. Gavazzi, G. Sun, and S. G. McNulty (2010), Hydraulic redistribution of soil water by roots affects whole-stand evapotranspiration and net ecosystem carbon exchange, *The New Phytologist*, *187*(1), 171–183, doi:10.1111/j.1469-8137.2010.03245.x.

Drake, J., S. Power, R. Duursma, B. Medlyn, M. Aspinwall, B. Choat, D. Creek, D. Eamus, C. Maier, S. Pfautsch, R. Smith, M. Tjoelker, and D. Tissue (2017), Stomatal and nonstomatal limitations of photosynthesis for four tree species under drought: A comparison of model formulations, *Agricultural and Forest Meteorology*, *247*, 454 – 466, doi: https://doi.org/10.1016/j.agrformet.2017.08.026.

Egea, G., A. Verhoef, and P. L. Vidale (2011), Towards an improved and more flexible representation of water stress in coupled photosynthesis-stomatal conductance models, *Agricultural and Forest Meteorology*, *151*(10), 1370 – 1384, doi: https://doi.org/10.1016/j.agrformet.2011.05.019.

Entekhabi, D., E. G. Njoku, P. E. O'Neill, K. H. Kellogg, W. T. Crow, W. N. Edelstein, J. K. Entin, S. D. Goodman, T. J. Jackson, J. Johnson, J. Kimball, J. R. Piepmeier, R. D. Koster, N. Martin, K. C. McDonald, M. Moghaddam, S. Moran, R. Reichle, J. C. Shi, M. W. Spencer, S. W. Thurman, L. Tsang, and J. V. Zyl (2010), The soil moisture active passive (smap) mission, *Proceedings of the IEEE*, *98*(5), 704–716, doi:

10.1109/JPROC.2010.2043918.

Epila, J., N. J. De Baerdemaeker, L. L. Vergeynst, W. H. Maes, H. Beeckman, and K. Steppe (2017), Capacitive water release and internal leaf water relocation delay drought-induced cavitation in African Maesopsis eminii, *Tree Physiology*, *37*(4), 481–490, doi: 10.1093/treephys/tpw128.

Farquhar, G. D., S. von Caemmerer, and J. A. Berry (1980), A biochemical model of photosynthetic CO_2 assimilation in leaves of C_3 species, *Planta*, *149*(1), 78–90, doi: 10.1007/BF00386231.

Ficklin, D. L., and K. A. Novick (2017), Historic and projected changes in vapor pressure deficit suggest a continentalâĂŘscale drying of the United States atmosphere, *Journal of Geophysical Research: Atmospheres*, *122*(4), 2061–2079, doi:10.1002/2016JD025855.

Fisher, R. A., M. Williams, R. L. Do Vale, A. L. Da Costa, and P. Meir (2006), Evidence from Amazonian forests is consistent with isohydric control of leaf water potential, *Plant, Cell & Environment*, *29*(2), 151–165, doi:10.1111/j.1365-3040.2005.01407.x.

Fisher, R. A., M. Williams, A. L. D. Costa, Y. Malhi, R. F. D. Costa, S. Almeida, and P. Meir (2007), The response of an Eastern Amazonian rain forest to drought stress: results and modelling analyses from a throughfall exclusion experiment, *Global Change Biology*, *13*(11), 2361–2378, doi:10.1111/j.1365-2486.2007.01417.x.

Fisher, R. A., M. Williams, M. de Lourdes Ruivo, A. L. de Costa, and P. Meir (2008), Evaluating climatic and soil water controls on evapotranspiration at two Amazonian rainforest sites, *Agricultural and Forest Meteorology*, *148*(6), 850 – 861, doi: https://doi.org/10.1016/j.agrformet.2007.12.001.

Flexas, J., J. Bota, F. Loreto, G. Cornic, and T. D. Sharkey (2004), Diffusive and metabolic limitations to photosynthesis under drought and salinity in c3 plants, *Plant Biology*, *6*(3), 269–279, doi:10.1055/s-2004-820867.

Flexas, J., M. Ribas-Carbó, J. Bota, J. Galmés, M. Henkle, S. Martínez-Cañellas, and H. Medrano (2006), Decreased rubisco activity during water stress is not induced by decreased relative water content but related to conditions of low stomatal conductance and chloroplast CO2 concentration, *New Phytologist*, *172*(1), 73–82, doi:10.1111/j.1469-8137.2006.01794.x.

Flexas, J., M. M. Barbour, O. Brendel, H. M. Cabrera, M. CarriquÃŋ, A. DÃŋaz-Espejo, C. Douthe, E. Dreyer, J. P. Ferrio, J. Gago, A. GallÃľ, J. GalmÃľs, N. Kodama, H. Medrano, ÃIJlo Niinemets, J. J. Peguero-Pina, A. Pou, M. Ribas-CarbÃş, M. TomÃąs, T. Tosens, and C. R. Warren (2012), Mesophyll diffusion conductance to co2: An unappreciated central player in photosynthesis, *Plant Science*, *193-194*, 70 – 84, doi: https://doi.org/10.1016/j.plantsci.2012.05.009.

Franks, P. J., P. L. Drake, and R. H. Froend (2007), Anisohydric but isohydrodynamic: seasonally constant plant water potential gradient explained by a stomatal control mechanism incorporating variable plant hydraulic conductance, *Plant, Cell & Environment*, *30*(1), 19–30, doi:10.1111/j.1365-3040.2006.01600.x.

Friedlingstein, P., M. Meinshausen, V. K. Arora, C. D. Jones, A. Anav, S. K. Liddicoat, and R. Knutti (2014), Uncertainties in CMIP5 climate projections due to carbon cycle feedbacks, *Journal of Climate*, *27*(2), 511–526.

Fu, R., L. Yin, W. Li, P. A. Arias, R. E. Dickinson, L. Huang, S. Chakraborty, K. Fernandes, B. Liebmann, R. Fisher, and R. B. Myneni (2013), Increased dry-season length over southern Amazonia in recent decades and its implication for future climate projection, *Proceedings of the National Academy of Sciences of the United States of America*, *110*(45), 18,110–18,115.

Gentine, P., D. Entekhabi, A. Chehbouni, G. Boulet, and B. Duchemin (2007), Analysis of evaporative fraction diurnal behaviour, *Agricultural and Forest Meteorology*, *143*(1), 13 – 29, doi:https://doi.org/10.1016/j.agrformet.2006.11.002.

Gentine, P., D. Entekhabi, and J. Polcher (2011), The diurnal behavior of evaporative fraction in the soilâĂŞvegetationâĂŞatmospheric boundary layer continuum, *Journal of Hydrometeorology*, *12*(6), 1530–1546, doi:10.1175/2011JHM1261.1.

Gentine, P., M. Guérin, M. Uriarte, N. G. McDowell, and W. T. Pockman (2016), An allometry-based model of the survival strategies of hydraulic failure and carbon starvation, *Ecohydrology*, *9*(3), 529–546, doi:10.1002/eco.1654.

Grant, J., J.-P. Wigneron, R. D. Jeu, H. Lawrence, A. Mialon, P. Richaume, A. A. Bitar, M. Drusch, M. van Marle, and Y. Kerr (2016), Comparison of SMOS and AMSR-E vegetation optical depth to four MODIS-based vegetation indices, *Remote Sensing of Environment*, *172*, 87 – 100, doi:https://doi.org/10.1016/j.rse.2015.10.021.

Green, J. K., A. G. Konings, S. H. Alemohammad, J. Berry, D. Entekhabi, J. Kolassa, J.-E. Lee, and P. Gentine (2017), Regionally strong feedbacks between the atmosphere and terrestrial biosphere, *Nature Geoscience*, *10*(6), 410–414, doi:10.1038/ngeo2957.

Harley, P. C., R. B. Thomas, J. F. Reynolds, and B. R. Strain (1992), Modelling photosynthesis of cotton grown in elevated co2, *Plant Cell Environment*, *15*(3), 271–282, doi:10.1111/j.1365-3040.1992.tb00974.x.

Holbrook, N. M., E. T. Ahrens, M. J. Burns, and M. A. Zwieniecki (2001), In vivo observation of cavitation and embolism repair using magnetic resonance imaging, *Plant Physiology*, *126*(1), 27–31, doi:10.1104/pp.126.1.27.

Huntingford, C., P. Zelazowski, D. Galbraith, L. M. Mercado, S. Sitch, R. Fisher, M. Lomas, A. P. Walker, C. D. Jones, B. B. B. Booth, Y. Malhi, D. Hemming, G. Kay, P. Good, S. L. Lewis, O. L. Phillips, O. K. Atkin, J. Lloyd, E. Gloor, J. Zaragoza-castells, P. Meir, R. Betts, P. P. Harris, C. Nobre, J. Marengo, and P. M. Cox (2013), Simulated resilience of tropical rainforests to co2-induced climate change, *Nature Geoscience*, *6*(4), 268–273.

Jackson, R. B., J. Canadell, J. R. Ehleringer, H. A. Mooney, O. E. Sala, and E. D. Schulze (1996), A global analysis of root distributions for terrestrial biomes, *Oecologia*, *108*(3), 389–411, doi:10.1007/BF00333714.

Jackson, R. B., J. S. Sperry, and T. E. Dawson (2000), Root water uptake and transport: using physiological processes in global predictions, *Trends in Plant Science*, *5*(11), 482 – 488, doi:https://doi.org/10.1016/S1360-1385(00)01766-0.

Jinyun, T., R. W. J., and N. Jie (), Incorporating root hydraulic redistribution in clm4.5: Effects on predicted site and global evapotranspiration, soil moisture, and water storage, *Journal of Advances in Modeling Earth Systems*, *7*(4), 1828–1848, doi:10.1002/2015MS000484.

Joetzjer, E., C. Delire, H. Douville, P. Ciais, B. Decharme, R. Fisher, B. Christoffersen, J. C. Calvet, A. C. L. da Costa, L. V. Ferreira, and P. Meir (2014), Predicting the response of the Amazon rainforest to persistent drought conditions under current and future climates: a major challenge for global land surface models, *Geoscientific Model Development*, *7*(6), 2933–2950, doi:10.5194/gmd-7-2933-2014.

Kattge, J., S. DĂŅAz, S. Lavorel, I. C. Prentice, P. Leadley, G. BĂŰNisch, E. Garnier, M. Westoby, P. B. Reich, I. J. Wright, J. H. C. Cornelissen, C. Violle, S. P. Harrison, P. M. Van Bodegom, M. ReichSTEIN, B. J. Enquist, N. A. Soudzilovskaia, D. D. Ackerly, M. Anand, O. Atkin, M. Bahn, T. R. Baker, D. Baldocchi, R. Bekker, C. C. Blanco, B. Blonder, W. J. Bond, R. Bradstock, D. E. Bunker, F. Casanoves, J. Cavender-Bares, J. Q. Chambers, F. S. Chapin Iii, J. Chave, D. Coomes, W. K. Cornwell, J. M. Craine, B. H. Dobrin, L. Duarte, W. Durka, J. Elser, G. Esser, M. Estiarte, W. F. Fagan, J. Fang, F. FernĂĄNdez-MĂĽNdez, A. Fidelis, B. Finegan, O. Flores, H. Ford, D. Frank, G. T. Freschet, N. M. Fyllas, R. V. Gallagher, W. A. Green, A. G. Gutierrez, T. Hickler, S. I. Higgins, J. G. Hodgson, A. Jalili, S. Jansen, C. A. Joly, A. J. Kerkhoff, D. Kirkup, K. Kitajima, M. Kleyer, S. Klotz, J. M. H. Knops, K. Kramer, I. KĂĳHn, H. Kurokawa, D. Laughlin, T. D. Lee, M. Leishman, F. Lens, T. Lenz, S. L. Lewis, J. Lloyd, J. LlusiĂĂ, F. Louault, S. Ma, M. D. MaHECHA, P. MaNNING, T. MaSSAD, B. E. Medlyn, J. Messier, A. T. Moles, S. C. MĂĳLLer, K. Nadrowski, S. Naeem, Ã. Niinemets, S. NĂŰLlerT, A. NĂĳSke, R. Ogaya, J. Oleksyn, V. G. Onipchenko, Y. Onoda, J. OrdoĂŚEz, G. Overbeck, W. A. Ozinga, S. PatiĂŚO, S. Paula, J. G. Pausas, J. PeĂŚUelas, O. L. Phillips, V. Pillar, H. Poorter, L. Poorter, P. Poschlod, A. Prinzing, R. Proulx, A. Rammig, S. Reinsch, B. Reu, L. Sack, B. Salgado-Negret, J. Sardans, S. Shiodera, B. Shipley, A. Siefert, E. Sosinski, J.-F. Soussana, E. Swaine, N. Swenson, K. Thompson,

P. Thornton, M. Waldram, E. Weiher, M. White, S. White, S. J. Wright, B. Yguel, S. Za-
ehle, A. E. Zanne, and C. Wirth (2011), Try âĂŞ a global database of plant traits, *Global
Change Biology*, *17*(9), 2905–2935, doi:10.1111/j.1365-2486.2011.02451.x.

Klein, T., and S. Niu (2014), The variability of stomatal sensitivity to leaf water potential
across tree species indicates a continuum between isohydric and anisohydric behaviours,
Functional Ecology, *28*(6), 1313–1320, doi:10.1111/1365-2435.12289.

Konings, A. G., and P. Gentine (2017a), Global variations in ecosystem-scale isohydricity,
Global Change Biology, *23*(2), 891–905, doi:10.1111/gcb.13389.

Konings, A. G., M. Piles, K. RÃűtzer, K. A. McColl, S. K. Chan, and D. Entekhabi (2016),
Vegetation optical depth and scattering albedo retrieval using time series of dual-polarized
l-band radiometer observations, *Remote Sensing of Environment*, *172*, 178 – 189, doi:
https://doi.org/10.1016/j.rse.2015.11.009.

Konings, A. G., A. P. Williams, and P. Gentine (2017b), Sensitivity of grassland productivity
to aridity controlled by stomatal and xylem regulation, *Nature Geoscience*, *10*(4), 284–
288, doi:10.1038/ngeo2903.

Kotowska, M. M., D. Hertel, Y. A. Rajab, H. Barus, and B. Schuldt (2015), Patterns in hy-
draulic architecture from roots to branches in six tropical tree species from cacao agro-
forestry and their relation to wood density and stem growth, *Frontiers in Plant Science*, *6*,
191, doi:10.3389/fpls.2015.00191.

Lee, J.-E., R. S. Oliveira, T. E. Dawson, and I. Fung (2005), Root functioning modifies sea-
sonal climate, *Proceedings of the National Academy of Sciences of the United States of
America*, *102*(49), 17,576–17,581, doi:10.1073/pnas.0508785102.

Lemordant, L., P. Gentine, A. S. Swann, B. I. Cook, and J. Scheff (2018), Critical impact of
vegetation physiology on the continental hydrologic cycle in response to increasing co2,
Proceedings of the National Academy of Sciences, doi:10.1073/pnas.1720712115.

Lin, C., P. Gentine, Y. Huang, K. Guan, H. Kimm, and S. Zhou (2018), Diel ecosys-
tem conductance response to vapor pressure deficit is suboptimal and indepen-
dent of soil moisture, *Agricultural and Forest Meteorology*, *250-251*, 24 – 34, doi:
https://doi.org/10.1016/j.agrformet.2017.12.078.

Mackay, D. S., D. E. Roberts, B. E. Ewers, J. S. Sperry, N. G. McDowell, and W. T. Pock-
man (2015), Interdependence of chronic hydraulic dysfunction and canopy processes can
improve integrated models of tree response to drought, *Water Resources Research*, *51*(8),
6156–6176, doi:10.1002/2015WR017244.

Manzoni, S., G. Vico, G. Katul, P. A. Fay, W. Polley, S. Palmroth, and A. Porporato (2011),
Optimizing stomatal conductance for maximum carbon gain under water stress: a meta-
analysis across plant functional types and climates, *Functional Ecology*, *25*(3), 456–467,
doi:10.1111/j.1365-2435.2010.01822.x.

Manzoni, S., G. Vico, G. Katul, S. Palmroth, R. B. Jackson, and A. Porporato (2013a), Hy-
draulic limits on maximum plant transpiration and the emergence of the safety-efficiency
trade-off, *New Phytologist*, *198*(1), 169–178, doi:10.1111/nph.12126.

Manzoni, S., G. Vico, S. Palmroth, A. Porporato, and G. Katul (2013b), Optimization of
stomatal conductance for maximum carbon gain under dynamic soil moisture, *Advances
in Water Resources*, *62*, 90 – 105, doi:https://doi.org/10.1016/j.advwatres.2013.09.020.

McDowell, N., C. D. Allen, â. K. Anderson, P. Brando, R. Brienen, J. Chambers, B. Christof-
fersen, S. Davies, C. Doughty, A. Duque, F. EspiritoâĂŘSanto, R. Fisher, C. G. Fontes,
D. Galbraith, D. Goodsman, C. Grossiord, H. Hartmann, J. Holm, D. J. Johnson, A. R.
Kassim, M. Keller, C. Koven, L. Kueppers, T. Kumagai, Y. Malhi, S. M. McMahon,
M. Mencuccini, P. Meir, P. Moorcroft, â. H. C. Muller, O. L. Phillips, T. Powell, C. A.
Sierra, J. Sperry, J. Warren, C. Xu, and X. Xu (2018), Drivers and mechanisms of tree
mortality in moist tropical forests, *New Phytologist*, *0*(0), doi:10.1111/nph.15027.

Mcdowell, N. G., and C. D. Allen (2015), Darcy's law predicts widespread forest mortality
under climate warming, *Nature Climate Change*, *5*(7), 669–672.

McDowell, N. G., R. A. Fisher, C. Xu, J. C. Domec, T. HÃűlttÃď, D. S. Mackay, J. S. Sperry,
A. Boutz, L. Dickman, N. Gehres, J. M. Limousin, A. Macalady, J. MartÃŋnez-Vilalta,

M. Mencuccini, J. A. Plaut, J. OgÃĺe, R. E. Pangle, D. P. Rasse, M. G. Ryan, S. Sevanto, R. H. Waring, A. P. Williams, E. A. Yepez, and W. T. Pockman (2013), Evaluating theories of drought-induced vegetation mortality using a multimodelâĂŞexperiment framework, *New Phytologist*, *200*(2), 304–321, doi:10.1111/nph.12465.

McDowell, N. G., A. P. Williams, C. Xu, W. T. Pockman, L. T. Dickman, S. Sevanto, R. Pangle, J. Limousin, J. Plaut, D. S. Mackay, J. Ogee, J. C. Domec, C. D. Allen, R. A. Fisher, X. Jiang, J. D. Muss, D. D. Breshears, S. A. Rauscher, and C. Koven (2016), Multi-scale predictions of massive conifer mortality due to chronic temperature rise, *Nature Climate Change*, *6*, 295–300, doi:10.1038/nclimate2873.

Medlyn, B. E., R. A. Duursma, D. Eamus, D. S. Ellsworth, I. C. Prentice, C. V. M. Barton, K. Y. Crous, P. De Angelis, M. Freeman, and L. Wingate (2011), Reconciling the optimal and empirical approaches to modelling stomatal conductance, *Global Change Biology*, *17*(6), 2134–2144, doi:10.1111/j.1365-2486.2010.02375.x.

Meinzer, F. C., S. A. James, and G. Goldstein (2004), Dynamics of transpiration, sap flow and use of stored water in tropical forest canopy trees, *Tree Physiology*, *24*(8), 901–909, doi:10.1093/treephys/24.8.901.

Meinzer, F. C., D. M. Johnson, B. Lachenbruch, K. A. McCulloh, and D. R. Woodruff (2009), Xylem hydraulic safety margins in woody plants: coordination of stomatal control of xylem tension with hydraulic capacitance, *Functional Ecology*, *23*(5), 922–930, doi:10.1111/j.1365-2435.2009.01577.x.

Momen, M., J. D. Wood, K. A. Novick, R. Pangle, W. T. Pockman, N. G. McDowell, and A. G. Konings (2017), Interacting effects of leaf water potential and biomass on vegetation optical depth, *Journal of Geophysical Research: Biogeosciences*, *122*(11), 3031–3046, doi:10.1002/2017JG004145.

Nepstad, D. C., R. de Carvalho, Claudio, E. A. Davidson, P. H. Jipp, and e. al (1994), The role of deep roots in the hydrological and carbon cycles of amazonian forests and pastures, *Nature*, *372*(6507), 666.

Novick, K. A., D. L. Ficklin, P. C. Stoy, C. A. Williams, G. Bohrer, A. Oishi, S. A. Papuga, P. D. Blanken, A. Noormets, B. N. Sulman, R. L. Scott, L. Wang, and R. P. Phillips (2016a), The increasing importance of atmospheric demand for ecosystem water and carbon fluxes, *Nature Climate Change*, *6*(11), 1023–1027.

Novick, K. A., C. F. Miniat, and J. M. Vose (2016b), Drought limitations to leaf-level gas exchange: results from a model linking stomatal optimization and cohesion-tension theory, *Plant, Cell & Environment*, *39*(3), 583–596, doi:10.1111/pce.12657.

Oleson, K. W., D. M. Lawrence, G. B. Bonan, B. Drewniak, M. Huang, C. D. Koven, S. Levis, F. Li, W. J. Riley, Z. M. Subin, S. C. Swenson, P. E. Thornton, A. Bozbiyik, R. Fisher, C. L. Heald, E. Kluzek, J.-F. Lamarque, P. J. Lawrence, L. R. Leung, W. Lipscomb, S. Muszala, D. M. Ricciuto, W. Sacks, Y. Sun, J. Tang, and Z.-L. Yang (2013), Technical description of version 4.5 of the community land model (clm), NCAR Tech. Note NCAR/TN-503+STR, *National Center for Atmospheric Research, Boulder, Colorado, 420 pp.*, doi:10.5065/D6RR1W7M.

Oliveira, R. S., T. E. Dawson, S. S. O. Burgess, and D. C. Nepstad (2005), Hydraulic redistribution in three amazonian trees, *Oecologia*, *145*(3), 354–363, doi:10.1007/s00442-005-0108-2.

Powell, T. L., D. R. Galbraith, B. O. Christoffersen, A. Harper, H. M. A. Imbuzeiro, L. Rowland, S. Almeida, P. M. Brando, A. C. L. da Costa, M. H. Costa, N. M. Levine, Y. Malhi, S. R. Saleska, E. Sotta, M. Williams, P. Meir, and P. R. Moorcroft (2013), Confronting model predictions of carbon fluxes with measurements of amazon forests subjected to experimental drought, *New Phytologist*, *200*(2), 350–365, doi:10.1111/nph.12390.

Powell, T. L., W. J. K., O. A. A. R., C. A. C. Lola, S. S. R., M. Patrick, and M. P. R. (2018), Differences in xylem and leaf hydraulic traits explain differences in drought tolerance among mature amazon rainforest trees, *Global Change Biology*, *23*(10), 4280–4293, doi:10.1111/gcb.13731.

Restaino, C. M., D. L. Peterson, and J. Littell (2016), Increased water deficit decreases douglas fir growth throughout western US forests, *Proceedings of the National Academy of Sciences*, *113*(34), 9557–9562, doi:10.1073/pnas.1602384113.

Restrepo-Coupe, N., N. M. Levine, B. O. Christoffersen, L. P. Albert, J. Wu, M. H. Costa, D. Galbraith, H. Imbuzeiro, G. Martins, A. C. da Araujo, Y. S. Malhi, X. Zeng, P. Moorcroft, and S. R. Saleska (2017), Do dynamic global vegetation models capture the seasonality of carbon fluxes in the amazon basin? A data-model intercomparison, *Global Change Biology*, *23*(1), 191–208, doi:10.1111/gcb.13442.

Rogers, A., B. E. Medlyn, J. S. Dukes, G. Bonan, S. Caemmerer, M. C. Dietze, J. Kattge, A. D. B. Leakey, L. M. Mercado, Ã. Niinemets, I. C. Prentice, S. P. Serbin, S. Sitch, D. A. Way, and S. Zaehle (2017), A roadmap for improving the representation of photosynthesis in earth system models, *New Phytologist*, *213*(1), 22–42, doi:10.1111/nph.14283.

Sack, L., P. J. Melcher, M. A. Zwieniecki, and N. M. Holbrook (2002), The hydraulic conductance of the angiosperm leaf lamina: a comparison of three measurement methods, *Journal of Experimental Botany*, *53*(378), 2177–2184.

Scholz, F. G., N. G. Phillips, S. J. Bucci, F. C. Meinzer, and G. Goldstein (2011), Hydraulic capacitance: Biophysics and functional significance of internal water sources, in Meinzer, F.C., Lachenbruch, B., Dawson, T. E. (eds) *Size- and Age-Related Changes in Tree Structure and Function*, pp. 341–361, Springer, Dordrecht.

Seager, R., A. Hooks, A. P. Williams, B. Cook, J. Nakamura, and N. Henderson (2015), Climatology, variability, and trends in the u.s. vapor pressure deficit, an important fire-related meteorological quantity, *Journal of Applied Meteorology and Climatology*, *54*(6), 1121–1141, doi:10.1175/JAMC-D-14-0321.1.

Sellers, P. J., D. A. Randall, G. J. Collatz, J. A. Berry, C. B. Field, D. A. Dazlich, C. Zhang, G. D. Collelo, and L. Bounoua (1996a), a revised land surface parameterization (sib2) for atmospheric gcms. part i: Model formulation, *Journal of Climate*, *9*(4), 676–705, doi:10.1175/1520-0442(1996)009<0676:ARLSPF>2.0.CO;2.

Sellers, P. J., C. J. Tucker, G. J. Collatz, S. O. Los, C. O. Justice, D. A. Dazlich, and D. A. Randall (1996b), A revised land surface parameterization (sib2) for atmospheric gcms. part ii: The generation of global fields of terrestrial biophysical parameters from satellite data, *Journal of Climate*, *9*(4), 706–737, doi:10.1175/1520-0442(1996)009<0706:ARLSPF>2.0.CO;2.

Sheffield, J., E. F. Wood, and M. L. Roderick (2012), Little change in global drought over the past 60 years, *Nature*, *491*(7424), 435–8.

Simonin, K. A., E. Burns, B. Choat, M. M. Barbour, T. E. Dawson, and P. J. Franks (2015), Increasing leaf hydraulic conductance with transpiration rate minimizes the water potential drawdown from stem to leaf, *Journal of Experimental Botany*, *66*(5), 1303–1315, doi:10.1093/jxb/eru481.

Siqueira, M., G. Katul, and A. Porporato (2008), Onset of water stress, hysteresis in plant conductance, and hydraulic lift: Scaling soil water dynamics from millimeters to meters, *Water Resources Research*, *44*(1), W01,432, doi:10.1029/2007WR006094.

Sperry, J. S., and D. M. Love (2015), What plant hydraulics can tell us about responses to climate-change droughts, *New Phytologist*, *207*(1), 14–27, doi:10.1111/nph.13354.

Sperry, J. S., F. R. Adler, G. S. Campbell, and J. P. Comstock (1998), Limitation of plant water use by rhizosphere and xylem conductance: results from a model, *Plant Cell Environment*, *21*(4), 347–359, doi:10.1046/j.1365-3040.1998.00287.x.

Sperry, J. S., U. G. Hacke, R. Oren, and J. P. Comstock (2002), Water deficits and hydraulic limits to leaf water supply, *Plant, Cell & Environment*, *25*(2), 251–263, doi:10.1046/j.0016-8025.2001.00799.x.

Sperry, J. S., M. D. Venturas, W. R. L. Anderegg, M. Mencuccini, D. S. Mackay, Y. Wang, and D. M. Love (2017), Predicting stomatal responses to the environment from the optimization of photosynthetic gain and hydraulic cost, *Plant, Cell & Environment*, *40*(6), 816–830, doi:10.1111/pce.12852, pCE-16-0541.R1.

Thornton, P. E., and N. E. Zimmermann (2007), An improved canopy integration scheme for a land surface model with prognostic canopy structure, *Journal of Climate*, *20*(15), 3902–3923, doi:10.1175/JCLI4222.1.

Trugman, A. T., D. Medvigy, J. S. Mankin, and W. R. L. Anderegg (2018), Soil moisture stress as a major driver of carbon cycle uncertainty, *Geophysical Research Letters*, *45*, doi:10.1029/2018GL078131.

Tyree, M. T., and J. S. Sperry (1988), Do woody plants operate near the point of catastrophic xylem dysfunction caused by dynamic water stress?: Answers from a model, *Plant Physiology*, *88*(3), 574–580.

Tyree, M. T., and J. S. Sperry (1989), Vulnerability of xylem to cavitation and embolism, *Annual Review of Plant Physiology and Plant Molecular Biology*, *40*(1), 19–36, doi:10.1146/annurev.pp.40.060189.000315.

Ukkola, A. M., M. G. D. Kauwe, A. J. Pitman, M. J. Best, G. Abramowitz, V. Haverd, M. Decker, and N. Haughton (2016), Land surface models systematically overestimate the intensity, duration and magnitude of seasonal-scale evaporative droughts, *Environmental Research Letters*, *11*(10), 104,012.

Verhoef, A., and G. Egea (2014), Modeling plant transpiration under limited soil water: Comparison of different plant and soil hydraulic parameterizations and preliminary implications for their use in land surface models, *Agricultural and Forest Meteorology*, *191*, 22–32, doi:https://doi.org/10.1016/j.agrformet.2014.02.009.

Warren, J. M., P. J. Hanson, C. M. Iversen, J. Kumar, A. P. Walker, and S. D. Wullschleger (2015), Root structural and functional dynamics in terrestrial biosphere models âĂŞ evaluation and recommendations, *New Phytologist*, *205*(1), 59–78, doi:10.1111/nph.13034.

Williams, A. P., C. D. Allen, A. K. Macalady, D. Griffin, C. A. Woodhouse, D. M. Meko, T. W. Swetnam, S. A. Rauscher, R. Seager, H. Grissino-Mayer, J. S. Dean, E. R. Cook, C. Gangodagamage, M. Cai, and N. G. Mcdowell (2013), Temperature as a potent driver of regional forest drought stress and tree mortality, *Nature Climate Change*, *3*(3), 292–297.

Williams, M., E. B. Rastetter, D. N. Fernandes, M. L. Goulden, S. C. Wofsy, G. R. Shaver, J. M. Melillo, J. W. Munger, S.-M. Fan, and K. J. Nadelhoffer (1996), Modelling the soil-plant-atmosphere continuum in a quercusâĂŞacer stand at harvard forest: the regulation of stomatal conductance by light, nitrogen and soil/plant hydraulic properties, *Plant, Cell & Environment*, *19*(8), 911–927, doi:10.1111/j.1365-3040.1996.tb00456.x.

Williams, M., B. E. Law, P. M. Anthoni, and M. H. Unsworth (2001), Use of a simulation model and ecosystem flux data to examine carbonâĂŞwater interactions in ponderosa pine., *Tree Physiology*, *21*(5), 287 – 298.

Xu, X., D. Medvigy, J. S. Powers, J. M. Becknell, and K. Guan (2016), Diversity in plant hydraulic traits explains seasonal and inter-annual variations of vegetation dynamics in seasonally dry tropical forests, *New Phytologist*, *212*(1), 80–95, doi:10.1111/nph.14009, 2015-20772.

Zhou, S., R. A. Duursma, B. E. Medlyn, J. W. Kelly, and I. C. Prentice (2013), How should we model plant responses to drought? An analysis of stomatal and non-stomatal responses to water stress, *Agricultural and Forest Meteorology*, *182-183*, 204 – 214, doi:https://doi.org/10.1016/j.agrformet.2013.05.009.

Zhou, S., B. Medlyn, S. Sabaté, D. Sperlich, I. C. Prentice, and D. Whitehead (2014), Short-term water stress impacts on stomatal, mesophyll and biochemical limitations to photosynthesis differ consistently among tree species from contrasting climates, *Tree Physiology*, *34*(10), 1035, doi:10.1093/treephys/tpu072.